URANIUM MINERALOGY OF THE NOPAL I NATURAL ANALOG SITE, CHIHUAHUA, MEXICO

Prepared for

Nuclear Regulatory Commission
Contract NRC-02-88-005

Prepared by

Center for Nuclear Waste Regulatory Analyses
San Antonio, Texas

June 1993

CNWRA 93-012

URANIUM MINERALOGY OF THE NOPAL I NATURAL ANALOG SITE, CHIHUAHUA, MEXICO

Prepared for

Nuclear Regulatory Commission
Contract NRC-02-88-005

Prepared by

English C. Pearcy
James D. Prikryl
William M. Murphy
Bret W. Leslie

Center for Nuclear Waste Regulatory Analyses
San Antonio, Texas

June 1993

ABSTRACT

At the Nopal I uranium deposit, primary uraninite (nominally UO_{2+x}) has altered almost completely to a suite of secondary uranyl minerals. The deposit is located in a Basin and Range horst composed of welded silicic tuff; uranium mineralization presently occurs in a chemically oxidizing and hydrologically unsaturated zone of the structural block. These characteristics are similar to those of the proposed United State high-level nuclear waste (HLW) repository at Yucca Mountain, Nevada. Petrographic analyses indicate that residual Nopal I uraninite is fine grained (5 to 10 μm) and has a low trace element content (average about 3 weight percent). These characteristics compare well with spent nuclear fuel. The oxidation and formation of secondary minerals from the uraninite have occurred in an environment dominated by components common in host rocks of the Nopal I system (e.g., Si, Ca, K, Na, and H_2O) and also common to Yucca Mountain. In contrast, secondary phases in most other uranium deposits form from elements largely absent from spent fuel and from the Yucca Mountain environment (e.g., Pb, P, and V). The oxidation of Nopal I uraninite and the sequence of alteration products, their intergrowths, and morphologies are remarkably similar to those observed in reported corrosion experiments using spent fuel and unirradiated UO_2 under conditions intended to approximate those anticipated for the proposed Yucca Mountain repository. The end products of these reported laboratory experiments and the natural alteration of Nopal I uraninite are dominated by uranophane [nominally $Ca(UO_2)_2Si_2O_7 \cdot 6H_2O$] with lesser amounts of soddyite [nominally $(UO_2)_2SiO_4 \cdot 2H_2O$] and other uranyl minerals. These similarities in reaction product occurrence developed despite the differences in time and physical-chemical environment between Yucca Mountain-approximate laboratory experiments and Yucca Mountain-approximate uraninite alteration at Nopal I, suggesting that the results may reasonably represent phases likely to form during long-term alteration of spent fuel in a Yucca Mountain repository. From this analogy, it may be concluded that the likely compositional ranges of dominant spent fuel alteration phases in the Yucca Mountain environment may be relatively limited and may be insensitive to small variations in system conditions.

CONTENTS

FIGURES

TABLES

ACKNOWLEDGMENTS

The authors appreciate the help received during this study from numerous colleagues. To the authors' knowledge, Philip C. Goodell was the first person to recognize the similarities between the Nopal I deposit and the proposed United States high level nuclear waste repository at Yucca Mountain. We are indebted to him for bringing Nopal I to our attention and for introducing us to the area. Ignacio Reyes provided indispensable information on the geology of the Peña Blanca district and the Nopal I deposit. Linda Kovach thoughtfully reviewed this study during its development and guided the authors in the use of natural analog data. Xavier Altamirano introduced the authors to the study area and made them aware of information developed during the URAMEX exploration of the Peña Blanca district. Robert Finch provided encouragement and insights into the subtleties of uranium mineralogy. Ronald Green developed the hydrologic data on the Peña Blanca district and the Nopal I deposit. Analytical work in support of this project was provided by Peggy Hunka, Renald Guillemette, William Nash, Harold Saldana, Ron McInnis, and Ramsey Railsback.

This paper was prepared to document work performed by the Center for Nuclear Waste Regulatory Analyses (CNWRA) for the U.S. Nuclear Regulatory Commission (NRC) under Contract No. NRC-02-88-005. The activities reported here were performed on behalf of the NRC Office of Nuclear Regulatory Research, Division of Regulatory Applications. This paper is an independent product of the CNWRA and does not necessarily reflect the views or regulatory position of the NRC.

1 INTRODUCTION

The U.S. Nuclear Waste Policy Act of 1982 (NWPA), as amended in 1987, designated Yucca Mountain, Nevada, as the sole candidate site to be characterized for possible permanent disposal of high-level nuclear waste (HLW) in the United States. On a total activity basis, most HLW that may be placed in a Yucca Mountain repository consists of spent fuel from commercial nuclear reactors. The alteration products that form as a result of spent fuel degradation in a geologic repository are important controls on radionuclide solubilities, on the source term for radionuclide release, and on potential transport phenomena. Though the oxidation of spent fuel has been considered theoretically (e.g., Shoesmith and Sunder, 1992) and has been studied in numerous laboratory experiments (e.g., Einziger et al., 1992), the composition, form, sequence, and relative importance of alteration products that would form during long-term reaction (e.g., 10^3 to 10^6 years) of spent fuel at Yucca Mountain remain a subject of significant uncertainty.

It is widely recognized that natural uraninite is a good analog material for comparison to aspects of spent nuclear fuel (e.g., Bates et al., 1990; Finch and Ewing, 1989; Janeczek and Ewing, 1992; Wronkiewicz et al., 1992). Previous natural analog studies of the alteration of natural uraninite cover a wide range of geochemical conditions (Table 1-1). These and other deposits provide definition of general trends for natural alteration of uraninite. Though the first four deposits listed in Table 1-1 are ancient, only Alligator Rivers and Shinkolobwe have undergone extensive oxidative alteration of uraninite. The uranium mineral assemblages at Oklo have undergone only limited oxidation in some areas [e.g., the Mounana area (Gauthier-Lafaye and Weber, 1989)]. Similarly, the assemblages at Cigar Lake have remained in a reducing environment and have not developed the complex secondary mineralogies common to oxidized uranium deposits. In a synthesis of observations from many deposits, Frondel (1956) reported a characteristic oxidation sequence for uraninite consisting of uranium oxides, followed by uranyl oxyhydroxides and, finally, uranyl silicates. Though there is broad recognition of this general trend, specific alteration minerals at a locality are a function of local conditions and elemental availability and vary considerably from site to site. Most detailed natural analog studies of oxidized uranium deposits (e.g., Alligator Rivers and Shinkolobwe) have considered systems in which the mineralogy of secondary phases is determined substantially by the presence of elements (e.g., Pb and/or P or V) that are absent in significant amounts in spent nuclear fuel or in the environment of the proposed HLW repository at Yucca Mountain.

The Nopal I uranium deposit within the Peña Blanca district in Chihuahua, Mexico, offers a geochemical environment similar to that of the proposed repository horizon at Yucca Mountain. Both Yucca Mountain and the Nopal I deposit are located in semi-arid to arid climatic regions (Figure 1-1). The Nopal I deposit is part of a Basin and Range horst composed of Tertiary rhyolitic tuffs underlain by carbonate sedimentary rocks as is Yucca Mountain (Mesozoic carbonates at Nopal, Paleozoic cabonates at Yucca Mountain). Further, both the proposed Yucca Mountain repository horizon and the Nopal I deposit are located in the oxidizing, hydrologically unsaturated zone 100 m or more above the water table (Pearcy et al., 1991) (Figure 1-2). Earlier work characterizing the Nopal I deposit includes Calas, 1977; Cardenas-Flores, 1985; George-Aniel et al., 1985; Goodell, 1981; Ildefonse et al., 1990a; Leroy et al., 1987; Muller et al., 1990. Studies establishing similarities between Nopal I and the proposed Yucca Mountain repository include: Ildefonse et al., 1990b; Murphy and Pearcy, 1992; Murphy et al., 1991; Pearcy and Murphy, 1992. No known natural system in which uraninite alteration has been studied compares as closely to Yucca Mountain as Nopal I.

Table 1-1. Selected uraninite deposits studied as natural analogs to nuclear waste disposal systems

Location	Environment	Age	Dominant U Mineralogy	Reference
Alligator Rivers, Australia	hydrologically saturated quartz-chlorite schists/main ore body reducing, weathered zone oxidizing	1.6 Ga	uraninite, Pb uranyl oxides, uranyl phosphates	(e.g., Airey, 1986)
Shinkolobwe, Zaire	hydrologically unsaturated dolomitic and chloritic sediments/oxidizing	1.8 Ga	uraninite, Pb uranyl oxides, uranyl silicates	(e.g., Finch and Ewing, 1991)
Oklo, Gabon	hydrologically saturated carbonaceous sandstones/main ore body reducing, weathered zone oxidizing	2.2 Ga	uraninite, uranyl vanadates, coffinite	(e.g., Curtis et al., 1981)
Cigar Lake, Canada	hydrologically saturated uraninite along a sandstone-schist/gneiss contact/reducing	1.3 Ga	uraninite, coffinite	(e.g., Cramer, 1986)
Osamu Utsumi, Brazil	hydrologically saturated phonolites and nepheline syenites/main ore body reducing, weathered zone oxidizing	>76 Ma	uraninite, brannerite	(e.g., Waber et al., 1991)
Peña Blanca, Mexico	hydrologically unsaturated rhyolitic tuffs/oxidizing	<44 Ma	uraninite, uranyl oxides, Ca uranyl silicates	this study

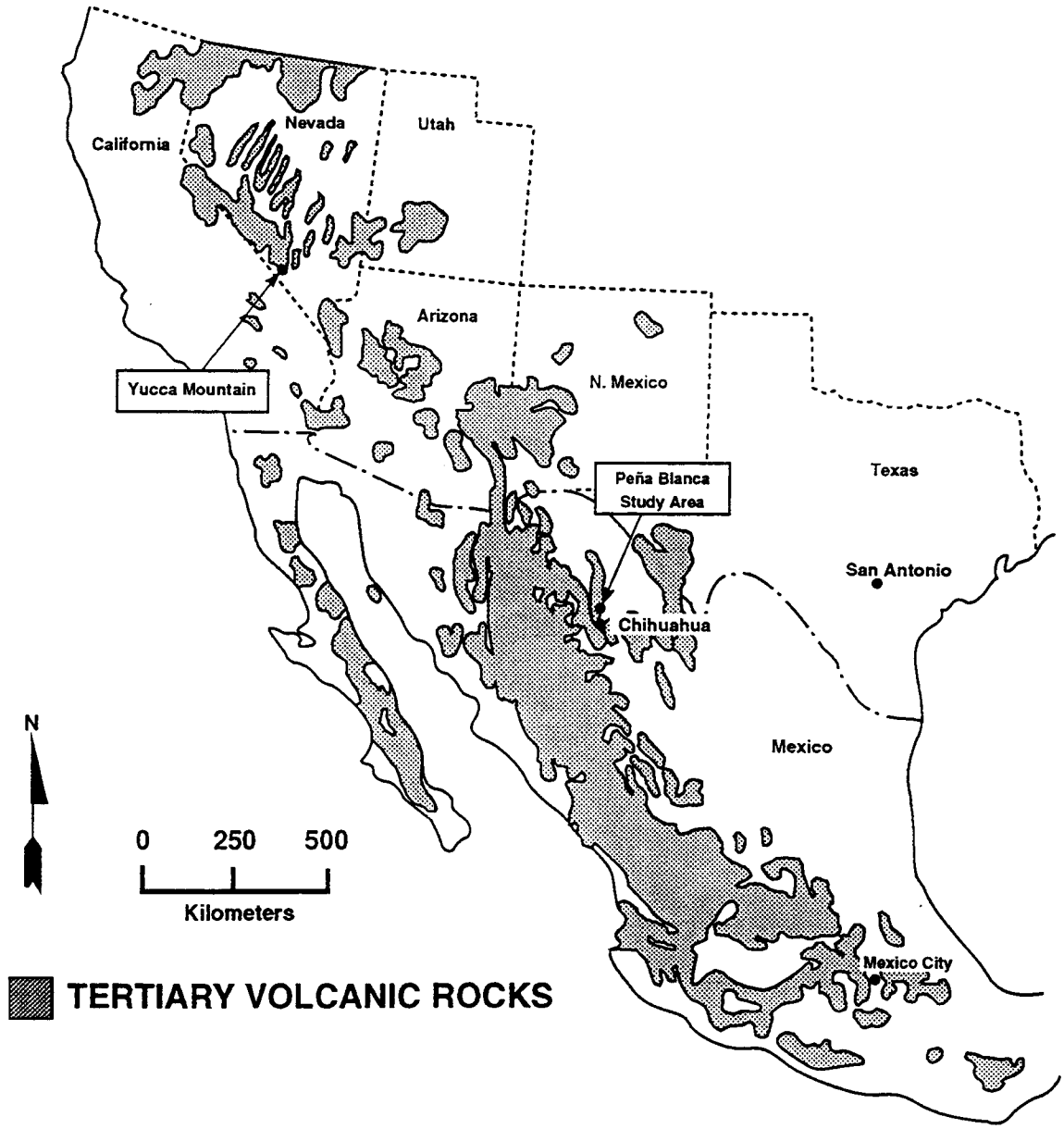

Figure 1-1. The Nopal I uranium deposit is located in the Peña Blanca mining district, Chihuahua, Mexico. Yucca Mountain, Nevada, the proposed site for the US high-level nuclear waste repository, is located northwest of the Peña Blanca district along a general trend of Tertiary volcanic rocks in the Basin and Range province.

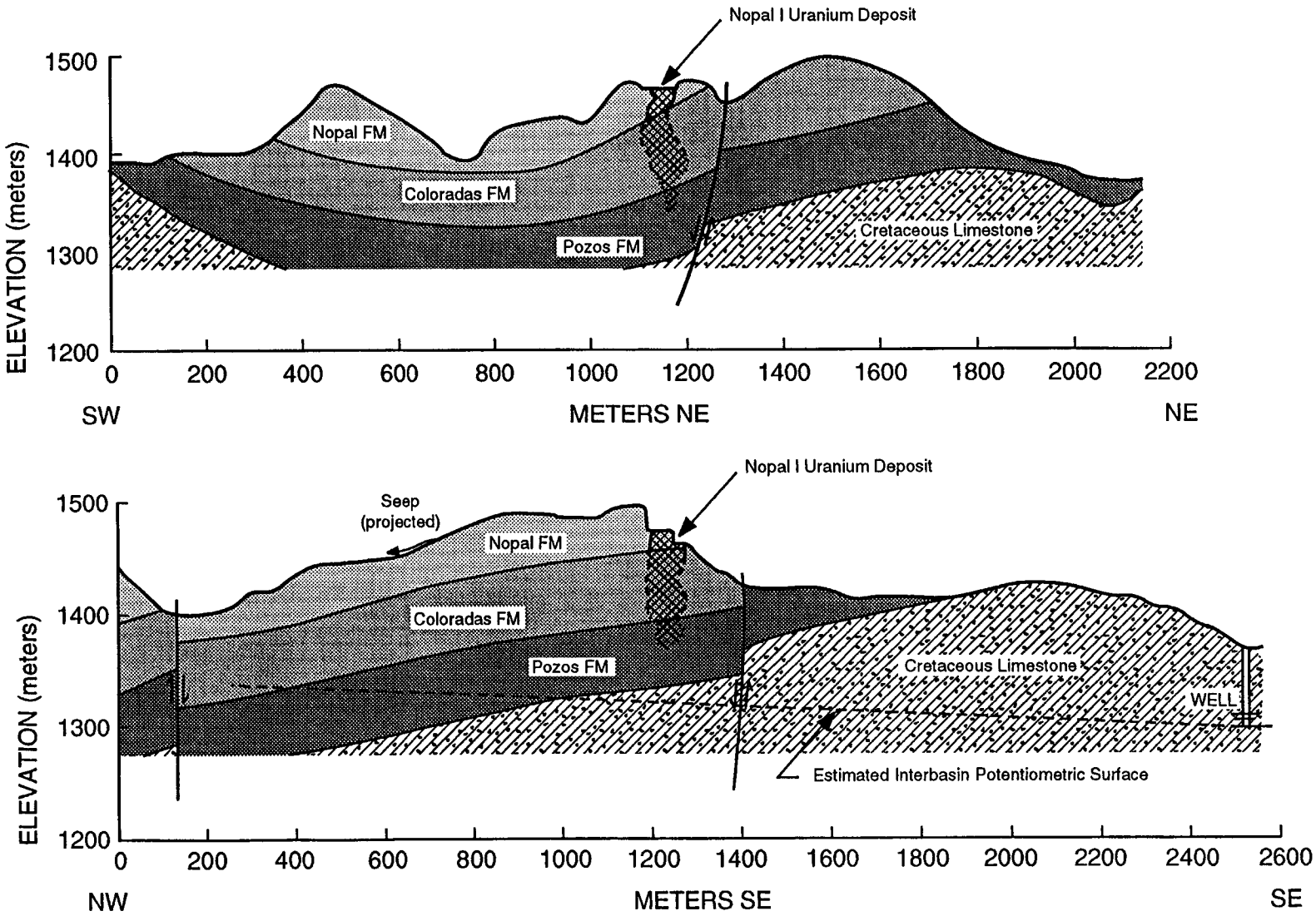

Figure 1-2. A vertical cross section of the Nopal I uranium deposit illustrates its location above the water table and within silicic tuffs of the Nopal and Coloradas Formations.

In addition to climatic, structural, hydrologic, and chemical similarities of the environments, the uraninite at Nopal I has a low trace element content. This chemical characteristic has resulted in formation of a sequence of secondary uranium minerals dominated by components common in host rocks of the Nopal I system and which are also common in the Yucca Mountain system (e.g., Si, Ca, and H_2O). In contrast, alteration minerals in most uranium deposits form from elements largely absent from spent fuel and from the Yucca Mountain environment (e.g., Pb, P, and V). Consequently, the Nopal I deposit presents a unique opportunity to study the alteration of uraninite over long time periods under conditions similar to those expected for a Yucca Mountain repository.

In this study, the alteration of uraninite (nominally UO_{2+x}) at the Nopal I uranium deposit is examined and compared to the spent fuel degradation processes expected in a Yucca Mountain repository environment. The mechanisms of alteration of uraninite at Nopal I and the nature and sequence of the resulting alteration products are compared to the results of laboratory oxidation experiments conducted using unirradiated UO_2 and spent fuel reported in the literature (Wilson, 1990a; Wilson, 1990b; Wilson, 1991; Wilson and Bruton, 1989; Bates et al., 1990; Wronkiewicz et al., 1992). The object of the comparison is to evaluate the degree to which relatively brief laboratory experiments (e.g., 1 to 10 years maximum duration) and/or long-term alteration of natural uraninite at Nopal I (e.g., 10^5 to 10^6 years), reflect the long-term behavior that may be expected of spent fuel in the proposed HLW repository at Yucca Mountain.

2 METHODS

Primary and secondary uranium phases at the Nopal I deposit were studied by optical petrography (OP), scanning electron microscopy/energy-dispersive x-ray analysis (SEM/EDS), x-ray diffractometry (XRD), and electron microprobe analysis (EMPA).

Optical microscopy was conducted using standard polished thin sections that were examined on a Nikon Optiphot-Pol transmitted/reflected light petrographic microscope. Polished section study was supplemented by examination of rock surfaces with a Nikon SMZ-2T binocular microscope; rock surfaces were broken to expose primary and secondary uranium mineralization. Higher resolution petrography employed an AMRAY Model 1645 SEM with a Tracor Northern Model 8502S EDS system for qualitative compositional analysis. Mineral identifications were confirmed using a Siemens D500 x-ray diffractometer with a Cu tube and Ni filter.

Quantitative mineral compositions were measured using a Cameca SX-50 electron microprobe. Standards used were: synthetic UO_2 for O and U; $NaAlSi_3O_8$ for Na; Al_2O_3 for Al; SiO_2 for Si; $Ca_5(PO_4)_3F$ for P; GaAs for As; ThO_2 for Th; PbS for Pb; $CaSiO_3$ for Ca; $KAlSi_3O_8$ for K; FeS_2 for Fe and S; $Mn_3Al_2(SiO_4)3$ for Mn; and TiO_2 for Ti. EMPA analytical conditions were: 30 nA beam current; 15 kV accelerating voltage; and 1 μm spot. A modified full matrix correction (PAP) for elements with long wavelength signals was used for data reduction.

3 RESULTS

Uranium minerals identified at Nopal I are listed in Table 3-1. The Nopal I deposit has fewer uranium minerals than most other uranium deposits that have undergone oxidative alteration of the primary mineral assemblage.

3.1 OCCURRENCE, TEXTURE, COMPOSITION, AND OXIDATION OF URANINITE

The uranium deposit at Nopal I is interpreted to have formed by hydrothermal solutions that precipitated uraninite as they moved through a highly fractured zone within welded silicic tuff. After formation of the primary uraninite, the deposit was altered to a suite of secondary minerals dominated by uranyl oxyhydroxides and uranyl silicates. It is likely that the secondary uranium minerals were formed by a combination of interaction with hydrothermal fluids and supergene alteration (George-Aniel et al., 1991). After deposition of the primary uraninite and possible subsequent hydrothermal alteration, the deposit was lifted above the water table by Basin and Range deformation. The deposit was exposed at the surface along the eastern face of a horst (Goodell, 1981). In this position, the deposit has been subject to weathering processes common to the desert areas of northern Mexico [i.e., annual rainfall of about 25 cm [U.S. Department of Commerce (USDOC) 1965], occurring in episodic downpours]. U-rich caliche located at the elevation of the deposit and about 3 m outside the limit of U mineral occurrence was dated during this study by a U-series isochron technique (Luo and Ku, 1991) at 53.6 $\pm$0.8 Ka, suggesting that weathering of the deposit has been the dominant mode of alteration for at least that period.

Field and petrographic relations at the Nopal I deposit indicate that uranium was originally precipitated as uraninite. Uraninite at Nopal I has only been observed preserved in a portion of the deposit consisting of a strongly silicified breccia. The uraninite-bearing breccia is composed of silicified, angular, tuff fragments cemented by a finely crystalline matrix (Figure 3-1). Breccia fragments juxtaposed with uraninite generally have maximum dimensions of several centimeters. Most uraninite occurs as a component of fracture-filling cement, with lesser amounts occurring as pore fillings within breccia fragments (Figure 3-1). Uraninite also replaces feldspar and ilmenite phenocrysts within silicified breccia fragments. Uraninite-bearing fractures are typically small, with maximum apertures of 1 to 2 mm. There is no evidence of symmetric precipitation of primary minerals within these uraninite-bearing veinlets; mineral compositions, crystal sizes, and crystal morphologies are approximately constant across the veinlets. Based on textural evidence, open spaces within breccia fragments originally occurred as intragranular pores with maximum dimensions of about 25 μm and as pores produced by dissolution of matrix feldspars with maximum dimensions of about 250 μm. These pores have largely been filled by primary and/or secondary uranium minerals.

Three texturally distinct forms of uraninite occur at Nopal I. Granular uraninite is the most abundant form and consists of a fine intergrowth (maximum crystal dimensions of 5 to 10 μm) of anhedral uraninite crystals and euhedral kaolinite (Figures 3-2 and 3-3). This fine-grained intergrowth has been referred to as pitchblende by previous workers at Nopal I (George-Aniel et al., 1991; George-Aniel et al., 1985). Granular uraninite that replaces phenocrysts within silicified breccia fragments tends to be relatively free of kaolinite, but is often intergrown with syngenetic, euhedral pyrite.

Colloform uraninite consists of aggregates of radial crystals that line formerly open spaces that are presently filled by secondary uranium phases (Figures 3-3 and 3-4). Individual sprays have maximum

Table 3-1. Uranium minerals identified at the Nopal I deposit

Mineral	Nominal Chemical Formula
Uraninite	UO_{2+x}
Soddyite	$(UO_2)_2SiO_4 \cdot 2H_2O$
Uranophane	$Ca(UO_2)_2Si_2O_7 \cdot 6H_2O$
Beta-uranophane	$Ca(UO_2)_2Si_2O_7 \cdot 6H_2O$
Weeksite	$K_2(UO_2)_2Si_6O_{15} \cdot 4H_2O$
Boltwoodite	$KH(UO_2)SiO_4 \cdot 1.5H_2O$
Becquerelite	$Ca(UO_2)_6O_4(OH)_6 \cdot 8H_2O$
Ianthinite	$U^{4+}(U^{6+}O_2)_5(OH)_{14} \cdot 3H_2O$
Schoepite	$UO_3 \cdot 2H_2O$
Dehydrated Schoepite	$UO_3 \cdot nH_2O$ $(n<2)$

radii of about 25 μm. Radial and concentric microfractures along which secondary uranium phases have formed are common within colloform crystal masses (Figure 3-4). However, colloform uraninite is free of kaolinite and pyrite. Textural relationships indicate that colloform uraninite was deposited after granular uraninite. Where granular uraninite does not completely fill fractures or open spaces, colloform uraninite has grown into the open spaces from the granular uraninite substrates, forming a distinctive rim (Figure 3-3). No uraninite has been observed that formed subsequent to colloform uraninite.

Granular and colloform uraninite are often observed growing on euhedral quartz substrates, including doubly terminated quartz crystals (Figures 3-3 and 3-4). It is probable that hydrothermal silicification produced the euhedral quartz overgrowths on pre-existing quartz crystals. The relationships among uraninite, euhedral quartz, and silicified host tuff suggest that silicification of the tuff occurred during the primary mineralizing event.

Euhedral uraninite is the least abundant uraninite form and consists of well-formed cubic crystals that fill intergranular pores within silicified breccia fragments. Like granular uraninite, euhedral uraninite is often intergrown or associated with syngenetic pyrite. In many instances, textural evidence indicates that uraninite replaces pyrite, for example, corroded pyrite crystals occur rimmed by uraninite.

X-ray diffraction (XRD) patterns of uraninite from Nopal I indicate that it has a low degree of crystallinity as evidenced by broad, diffuse peaks, suggesting varying degrees of oxidation. Where x-ray peak positions and intensities are discernible, the uraninite appears to consist predominantly of $UO_{2.25}$ with lesser amounts of $UO_{2.33}$. At $UO_{2.25}$, there is one extra oxygen per unit cell. Above $UO_{2.25}$ (Smith, 1984) or $UO_{2.33}$ (Johnson and Shoesmith, 1988), the ideal cubic structure is replaced by a tetragonal form as the original fluorite-type structure becomes increasingly distorted. Further oxidation to $UO_{2.67}$ results in an orthorhombic structure as the oxygen coordination changes to a 7-coordinated pentagonal dipyramid (Frondel, 1956).

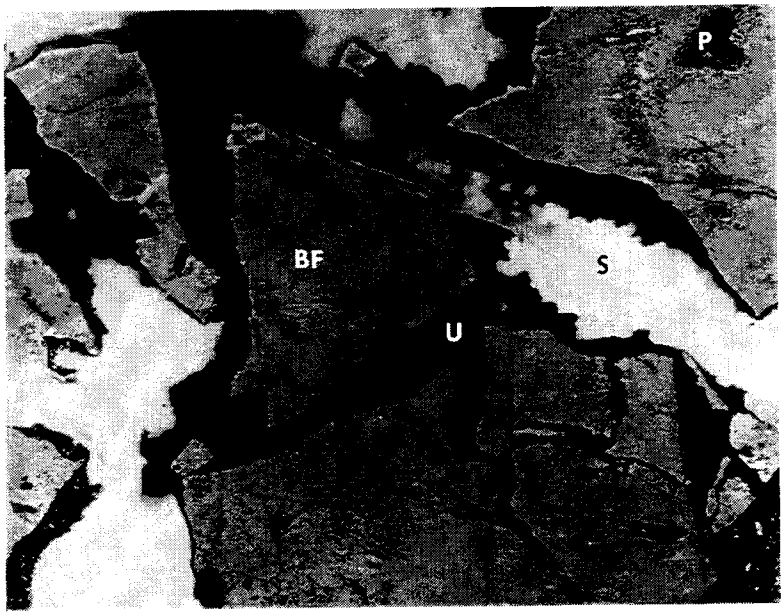

Figure 3-1. Photograph of silicified breccia fragments (BF) cemented by a black fine-crystalline matrix composed of uraninite (U) intergrown with kaolinite. Oxidation of the matrix uraninite has lead to the formation of uranyl silicates (S). Black areas within breccia fragments are feldspar and/or ilmenite phenocrysts (P) replaced by uraninite or intergranular pores filled by uraninite. Field of view is 1.2 mm.

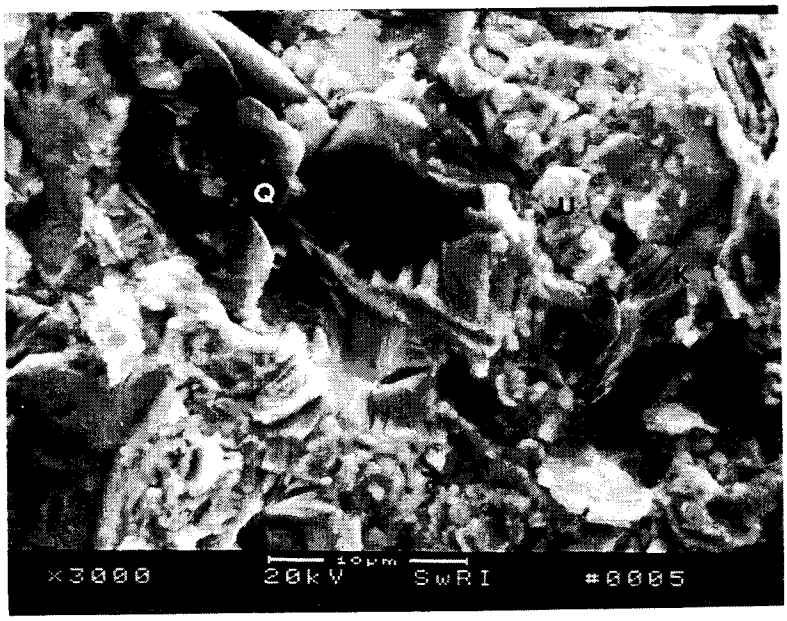

Figure 3-2. SEM photomicrograph of granular uraninite. Uraninite crystals (U) are intergrown with kaolinite (K). Euhedral quartz crystals (Q) are also present and act as substrates for uraninite.

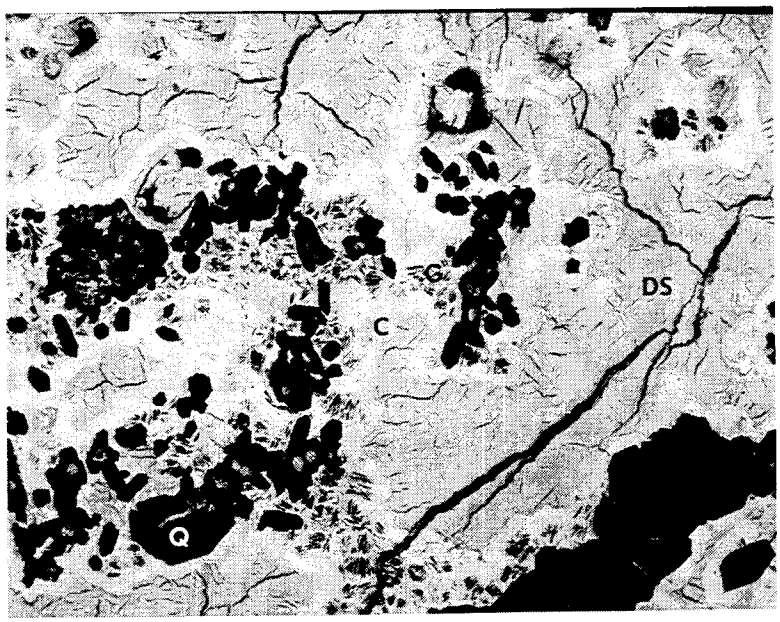

Figure 3-3. Backscattered electron photomicrograph of uranium phases filling pore space within a breccia fragment. Granular uraninite (G) is followed by colloform uraninite (C). Colloform uraninite forms a distinct rim which indicates the end of the primary mineralizing event. The remaining open space is filled by dehydrated schoepite (DS). Notice the euhedral quartz crystals (Q), some with double terminations, which act as substrates for uraninite. Field of view is 450 microns wide.

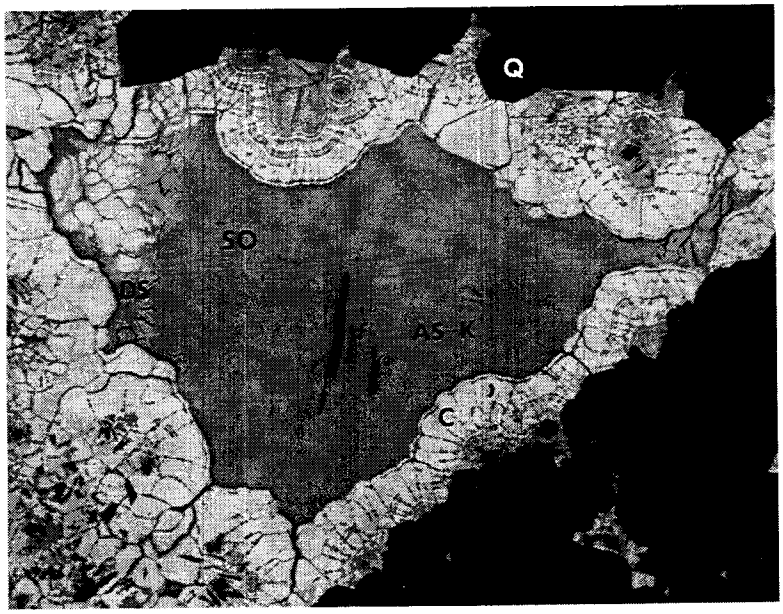

Figure 3-4. Backscattered electron photomicrograph of colloform uraninite (C) lining a fracture. Note euhedral quartz substrates (Q) and radial and concentric microfractures within colloform crystals. Corroded, dehydrated schoepite (DS) followed by soddyite (SO) and an As- and K-rich uranyl oxide hydrate (As-K) fill the remaining open space. Field of view is 125 microns wide.

Electron microprobe analyses (EMPA) of uraninite from Nopal I are given in Table 3-2. Analyses are grouped by the three uraninite forms. EMPA data provide indications of the significance of impurities in uraninite and the oxidation state of uranium. Impurities may be components in solid solution in the uraninite or discrete phases. Likely phases are kaolinite, feldspar, quartz, pyrite, and ilmenite. For the analyses listed in Table 3-2, there is no apparent correlation between the Al and Si contents, precluding dominant contamination with kaolinite. Similarly, no apparent correlation exists between the sum Na + K + 0.5Ca and either Si or Al, indicating that feldspar is not the dominant contaminating phase. Insignificance of contaminating ilmenite is indicated by a lack of correlation between Fe and Ti. A weak negative correlation between Fe and S argues against pyrite contamination.

The oxidation state of the uranium in Nopal I uraninite can be investigated by calculating the oxygen that is not required to balance the positive charge of impurities (i.e., the total measured oxygen minus the oxygen) associated with contaminants. Corrected oxygen contents were calculated assuming contaminant species to be in their most oxidized states (e.g., Fe^{3+} and S^{6+}), which tends to maximize the oxygen associated with these species and minimize the corrected oxygen content. However, species of ambiguous valence compose a small fraction of impurities in most analyses. The hydrogen content of the samples is unknown and was neglected, which tends to minimize the estimation of oxygen associated with impurities and maximize values of corrected oxygen.

The U concentration plotted against corrected O (Figure 3-5) shows U/O ratios to be scattered over a small range. U/O ratios corresponding to UO_2, $UO_{2.25}$, and $UO_{2.33}$ are plotted as lines in Figure 3-5. The data generally fall within this range, as expected from crystallographic constraints and XRD data. Data plotting at U contents in excess of the UO_2 line indicate underestimation of corrected oxygen (e.g., due to assignment of excess charge to species such as Fe and S) or errors in analytical data. A significant hydrogen content and an overestimation of residual oxygen is not generally indicated by the data. No significant difference is apparent in the ratio of corrected oxygen to uranium among the textural types of uraninite from Nopal I. Approximately half of the analyses yield corrected oxygen to uranium ratios between 2.15 and 2.25 (Figure 3-6).

The silica content of all uraninite samples is remarkably similar (Figure 3-7). Si contents in 37 analyses are 0.44 ± 0.12 (1σ) atom percent. This consistency suggests that Si occurs in a single phase (i.e., uraninite) at a chemical potential that was fixed by equilibrium with a silica phase (e.g., quartz) over a narrow temperature range. The K content of uraninites is also remarkably constant at 0.26 ± 0.04 (1σ) atom percent (37 samples), also suggesting uraninite formation at equilibrium with systems of constant (buffered) K chemical potential (Figure 3-7). However, there is no correlation between the K and Si contents of the samples.

Lead contents of Nopal I uraninite are low and highly variable, ranging from 0.04 to 6.73 weight percent, averaging 1.64 weight percent (0.02 to 2.66 atom percent, Figure 3-8). Pb in the uraninite was produced at least in part by radiogenic decay of U and Th. Quantitative microprobe analysis of uraninite allows the calculation of Pb-U,Th chemical dates of microareas (Hofmann and Eikenberg, 1991). The chemical Pb-U,Th method is based on the premise that all the Pb in a mineral is radiogenic in origin and that its amount increases as a function of time. The large uncertainty arising from the inability to clearly distinguish between nonradiogenic and radiogenic lead components and any possible gains or losses of U and Pb makes the interpretation of chemical Pb-U,Th dates of U minerals difficult. However, by assuming a closed system and the absence of nonradiogenic lead, Pb concentrations in Nopal I uraninites produce chemical Pb-U,Th mineral dates between about 4 to 580 Ma.

Table 3-2. Electron microprobe analyses of Nopal I uraninite (normalized to 100 atom percent)

Sample	U	O	Na	Al	Si	P	As	Th	Pb	Ca	K	S	Fe	Mn	Ti
Colloform Uraninite															
32-ts2-p1	32.34	66.42	0.11	0.01	0.33	0.00	0.03	0.01	0.05	0.00	0.24	0.20	0.00	0.01	0.06
32-ts2-p4	30.88	66.98	0.43	0.09	0.65	0.00	0.02	0.00	0.04	0.07	0.28	0.24	0.01	0.02	0.10
32-ts2-p5	33.78	64.65	0.16	0.31	0.34	0.03	0.01	0.00	0.02	0.04	0.26	0.16	0.02	0.00	0.03
32-ts2-p6	32.79	65.52	0.35	0.08	0.44	0.00	0.01	0.02	0.07	0.00	0.26	0.25	0.00	0.00	0.01
32-ts4-p2	29.75	66.86	0.85	0.16	0.32	0.02	0.15	0.01	0.58	0.65	0.26	0.16	0.04	0.00	0.00
32-ts4-p6	30.52	66.96	0.66	0.10	0.47	0.04	0.09	0.00	0.26	0.29	0.20	0.16	0.01	0.00	0.04
32-ts4-p19	29.61	68.38	0.32	0.07	0.46	0.00	0.06	0.02	0.28	0.07	0.28	0.21	0.00	0.03	0.00
32-ts4-p21	30.01	67.93	0.32	0.05	0.42	0.03	0.00	0.01	0.30	0.14	0.26	0.26	0.01	0.01	0.06
1-ts3-p1	30.28	68.09	0.17	0.12	0.45	0.00	0.04	0.01	0.05	0.00	0.26	0.27	0.01	0.02	0.03
1-ts3-p2	30.09	68.22	0.25	0.04	0.52	0.00	0.00	0.01	0.02	0.00	0.31	0.29	0.00	0.02	0.05
1-ts3-p6	30.76	67.44	0.20	0.17	0.58	0.00	0.00	0.00	0.03	0.01	0.32	0.21	0.02	0.00	0.07
30-ts2-p1	28.94	66.80	0.74	0.08	0.56	0.03	0.11	0.01	0.75	1.37	0.18	0.05	0.12	0.00	0.08
30-ts2-p2	29.05	67.46	0.60	0.00	0.50	0.04	0.13	0.01	0.61	1.03	0.22	0.04	0.09	0.00	0.03
30-ts2-p5	27.96	67.20	0.77	0.08	0.63	0.01	0.10	0.00	0.56	2.08	0.21	0.05	0.14	0.02	0.00
30-ts2-p6	27.65	69.22	0.58	0.06	0.42	0.00	0.07	0.00	0.57	0.82	0.29	0.09	0.08	0.03	0.02
30-ts2-p7	28.12	67.31	0.89	0.06	0.57	0.00	0.10	0.01	0.53	1.84	0.23	0.02	0.05	0.00	0.09
32-ts5-p5	27.65	68.69	0.91	0.22	0.31	0.06	0.10	0.01	0.51	0.85	0.27	0.07	0.06	0.00	0.08
32-ts5-p6	27.81	68.83	0.99	0.03	0.22	0.00	0.09	0.00	0.52	0.92	0.27	0.04	0.07	0.02	0.00
Average	29.89	67.39	0.52	0.09	0.46	0.01	0.06	0.01	0.32	0.56	0.26	0.15	0.04	0.01	0.04

Table 3-2 (cont'd). Electron microprobe analyses of Nopal I uraninite (normalized to 100 atom percent)

Sample	U	O	Na	Al	Si	P	As	Th	Pb	Ca	K	S	Fe	Mn	Ti
Granular Uraninite															
32-ts4-p18	27.15	67.28	0.67	0.12	0.42	0.06	0.09	0.00	2.66	1.04	0.22	0.00	0.06	0.05	0.01
32-ts4-p20	27.10	68.09	0.68	0.18	0.47	0.00	0.07	0.01	1.38	1.50	0.25	0.00	0.03	0.01	0.03
32-ts4-p23	27.66	67.54	0.75	0.16	0.45	0.01	0.06	0.00	1.34	1.46	0.28	0.02	0.07	0.00	0.01
32-ts4-p24	28.48	67.68	0.78	0.22	0.44	0.00	0.17	0.00	0.31	1.36	0.28	0.01	0.00	0.07	0.00
32-ts4-p25	28.44	67.41	0.92	0.14	0.37	0.03	0.20	0.00	0.39	1.52	0.25	0.02	0.06	0.01	0.05
32-ts4-p27	28.19	67.78	0.77	0.15	0.40	0.01	0.16	0.00	0.42	1.62	0.23	0.02	0.03	0.00	0.03
1-ts3-11	29.70	67.40	0.62	0.04	0.37	0.00	0.07	0.00	0.31	0.84	0.31	0.14	0.00	0.00	0.00
1-ts3-12	27.84	68.32	0.85	0.04	0.26	0.02	0.07	0.00	0.57	1.48	0.26	0.10	0.01	0.00	0.00
1-ts3-14	27.49	67.94	0.90	0.34	0.48	0.00	0.05	0.00	0.80	1.43	0.28	0.02	0.00	0.01	0.06
1-ts3-18	32.93	65.13	0.45	0.02	0.34	0.01	0.01	0.01	0.08	0.10	0.37	0.25	0.06	0.00	0.04
1-ts3-p19	31.82	66.70	0.29	0.02	0.32	0.01	0.00	0.00	0.05	0.02	0.30	0.11	0.08	0.00	0.08
Average	28.80	67.39	0.70	0.13	0.39	0.01	0.09	0.00	0.76	1.12	0.28	0.06	0.04	0.01	0.03

Table 3-2 (cont'd). Electron microprobe analyses of Nopal I uraninite (normalized to 100 atom percent)

Sample	U	O	Na	Al	Si	P	As	Th	Pb	Ca	K	S	Fe	Mn	Ti
Euhedral Uraninite															
32-ts2-p9	29.34	66.27	0.84	0.08	0.71	0.02	0.04	0.00	0.07	2.00	0.26	0.11	0.01	0.00	0.05
32-ts4-p1	27.42	66.71	1.43	0.08	0.48	0.02	0.14	0.00	1.04	2.14	0.20	0.00	0.13	0.00	0.02
32-ts4-p4	27.43	67.02	1.34	0.04	0.40	0.01	0.13	0.01	0.90	2.14	0.20	0.02	0.12	0.00	0.03
32-ts4-p8	27.43	66.87	1.48	0.11	0.39	0.08	0.17	0.00	0.75	2.07	0.25	0.00	0.20	0.01	0.00
1-ts3-p10	27.06	66.91	1.06	0.20	0.42	0.06	0.00	0.01	2.05	1.65	0.27	0.00	0.00	0.07	0.04
1-ts3-p15	29.03	66.28	0.86	0.32	0.68	0.01	0.06	0.00	0.78	1.26	0.35	0.03	0.03	0.04	0.08
32-ts5-p1	27.43	66.56	1.13	0.10	0.24	0.09	0.11	0.00	0.58	3.16	0.23	0.03	0.14	0.02	0.00
32-ts5-p2	27.59	66.54	1.10	0.09	0.31	0.01	0.09	0.00	0.68	2.82	0.29	0.02	0.22	0.01	0.04
Average	27.84	66.65	1.15	0.13	0.45	0.04	0.09	0.00	0.86	2.15	0.25	0.03	0.11	0.02	0.03

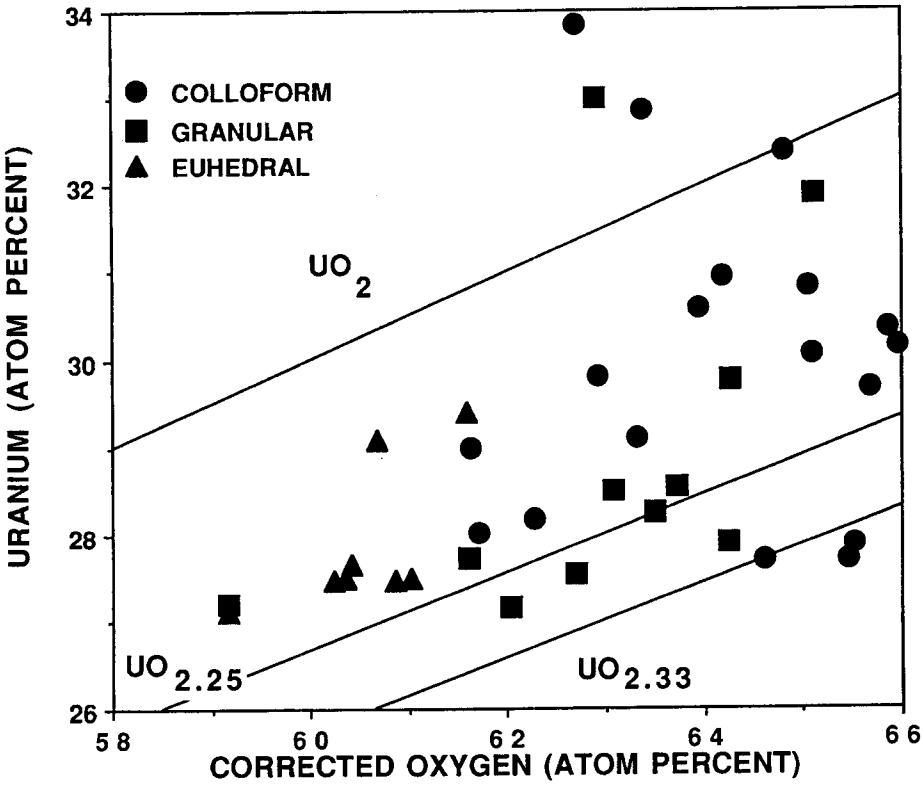

Figure 3-5. Microprobe data for the uranium content of uraninites from Nopal I as a function of the oxygen content not associated with contaminant species (corrected oxygen). Lines represent the range of U/O ratios of typical uraninites, 2 to 2.25 or 2.33. Uraninite textures are indicated by symbol shapes as indicated.

The upper end of this range is geologically untenable as the host rocks were formed 43.8 Ma ago (Alba and Chavez, 1974), and clearly indicates the presence of nonradiogenic lead in most of the samples (Pb atom percent > 0.21 produces dates >44 Ma). The observed range of uraninite Pb contents suggests that Pb was mobile in the Nopal I system during formation of the uraninite. In contrast to the young Nopal I deposit, Pb concentrations in uraninite of ancient (e.g., 10^9 years) uranium deposits may be 10 to 20 weight percent (Frondel, 1958).

An investigation of relations among uraninite analytical data revealed distinct negative correlations between the sulfur content of the uraninite samples and the concentrations of most major cationic contaminants, including Ca, Na, Pb, and Fe (Figures 3-7 and 3-8). Even As decreases slightly with increasing S. Colloform uraninite is relatively rich in S and poor in other cations, whereas euhedral uraninite tends to be poor in sulfur and rich in other cations. Granular uraninite spans the range of S and cation concentrations. The fairly constant concentrations of Si and K are essentially independent of the S content. Sulfur concentrations are low, ranging from below detection at less than 0.01 atom percent to 0.3 atom percent, indicating that the noted inverse correlations are not an artifact of normalization of totals to 100 percent. Nevertheless, S concentrations vary significantly among analyses by a factor of 30 or more. Concentrations of Ca, Na, Pb, and Fe also range over a factor of 15 to 30 or more. Positive correlations between cation concentrations (e.g., Na and Ca; Figure 3-9) correspond generally to their mutual inverse correlations to the S content. In contrast, the U concentration is positively

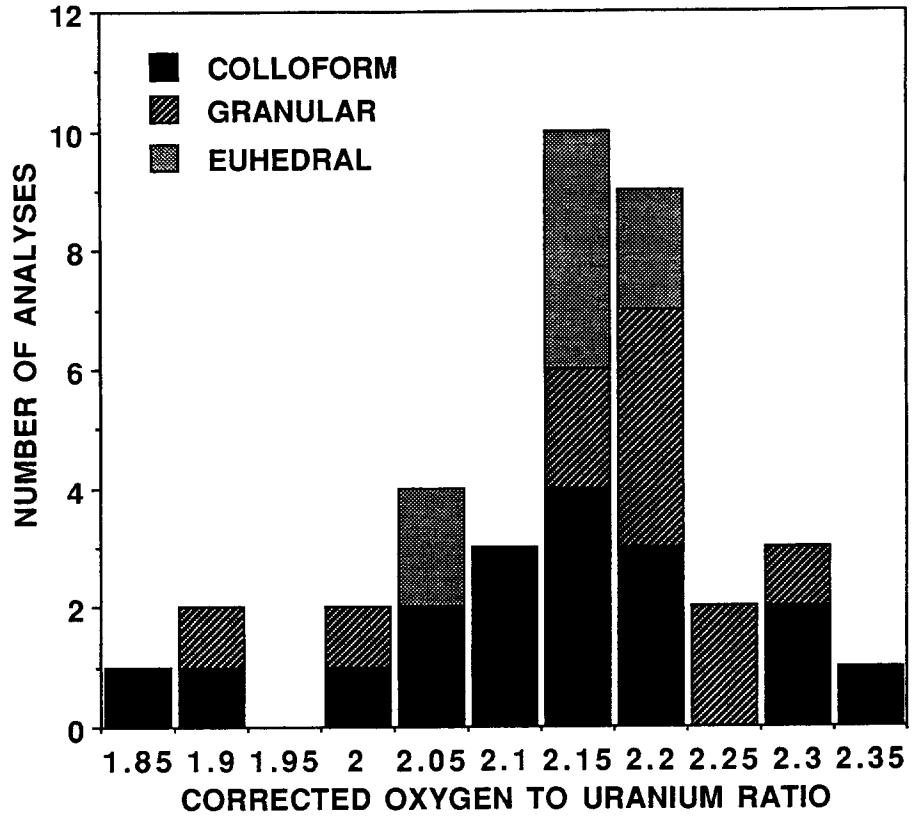

Figure 3-6. Histogram showing the number of analyses with ratios of corrected oxygen to uranium (on an atomic basis) in increments of 0.05. Each increment is labelled by the corrected O/U value at its lower end. For example, approximately half of the analyses fall in the range 2.15 to 2.25.

correlated with S (Figure 3-10), which is a reflection of higher U fractions in samples with lower fractions of cation impurities.

3.2 URANYL OXIDE HYDRATES

The initial products of oxidized uraninite dissolution at Nopal I are uranyl oxide hydrates including ianthinite, schoepite, and dehydrated schoepite. Uranyl oxide hydrates occur both as direct replacements of uraninite and as open space fillings, often overgrowing colloform uraninite. In samples containing multiple uranyl oxide phases, ianthinite is the earliest formed uranyl oxide hydrate and is followed by schoepite and/or dehydrated schoepite (Figure 3-11).

Ianthinite (nominally $U^{4+}(U^{6+}O_2)_5(OH)_{14} \cdot 3H_2O$), a uranyl oxide hydrate containing both U^{4+} and U^{6+}, is rarely preserved in most uranium deposits. It is, however, relatively common in uraninite-bearing specimens from Nopal I, where it generally occurs juxtaposed with granular uraninite as pseudomorphs after the uraninite. In other areas, ianthinite occurs as deep red to violet acicular crystals in cavities and fractures (Figure 3-11). Nopal I ianthinite is unstable in air; ianthinite samples progressively convert to schoepite over approximately 6 months exposure to ambient laboratory conditions. Occurrence of ianthinite at Nopal I demonstrates effective isolation of minerals from

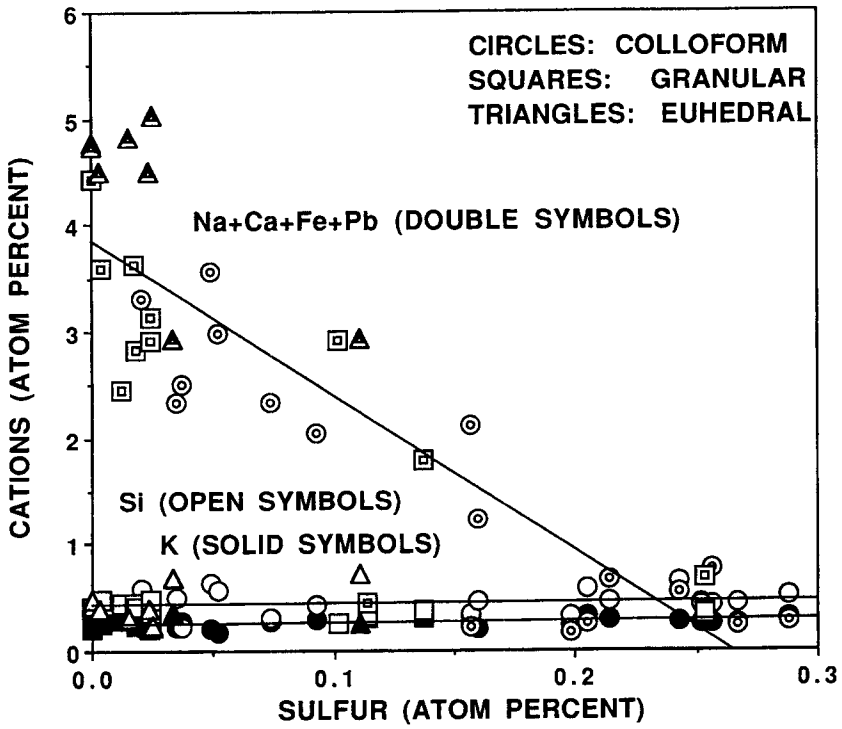

Figure 3-7. Cation contents in uraninite as a function of the sulfur content. Silicon is represented by open symbols, potassium by solid symbols, and the sum of sodium, calcium, iron, and lead is shown by double symbols. Uraninite textures are indicated by symbol shapes as indicated. The upper and lower near-horizontal lines are linear regressions of the Si and K contents, respectively. The diagonal line is a linear regression of the Na+Ca+Fe+Pb sum.

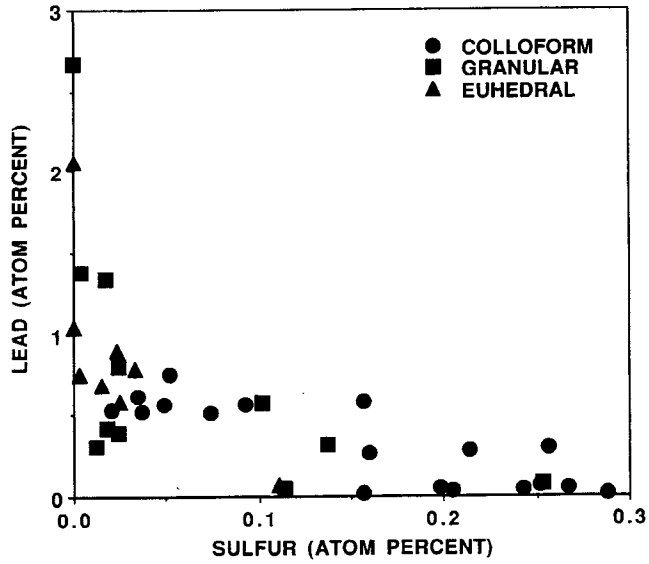

Figure 3-8. Lead contents in uraninite as a function of the sulfur content. Uraninite textures are indicated by symbol shapes as indicated.

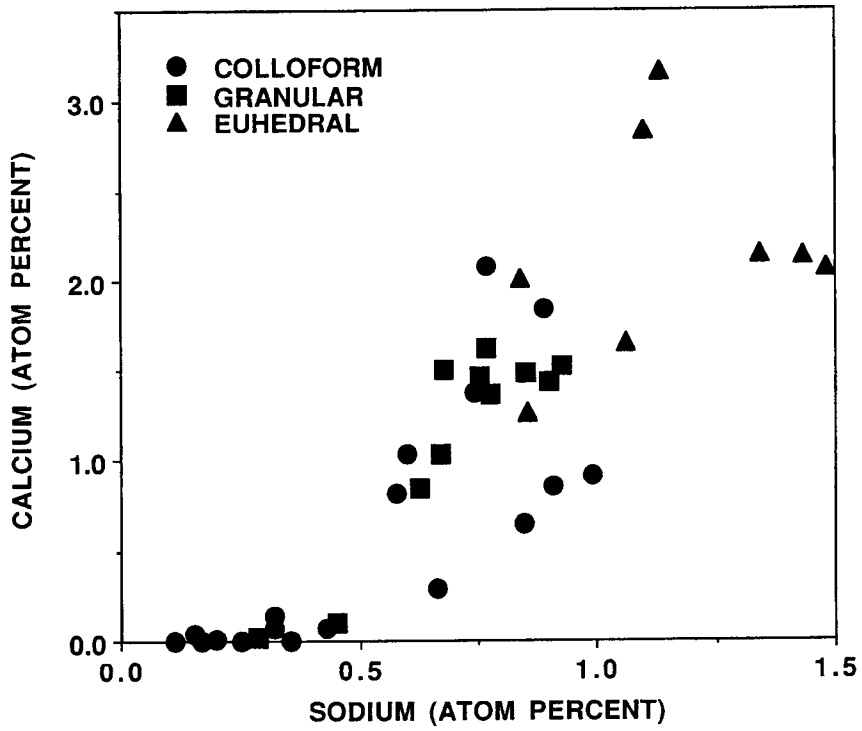

Figure 3-9. Calcium contents in uraninite as a function of the sodium content. Uraninite textures are indicated by symbol shapes as indicated.

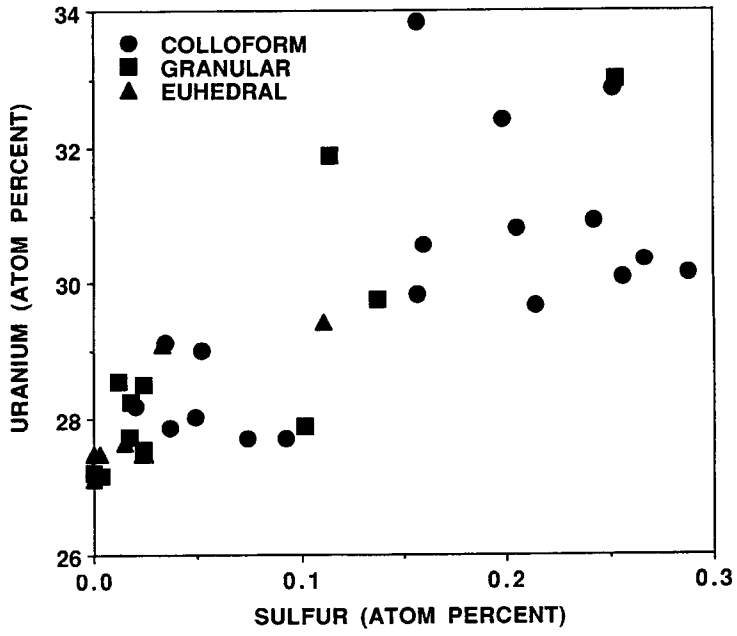

Figure 3-10. Uranium contents in uraninite as a function of the sulfur content. Uraninite textures are indicated by symbol shapes as indicated.

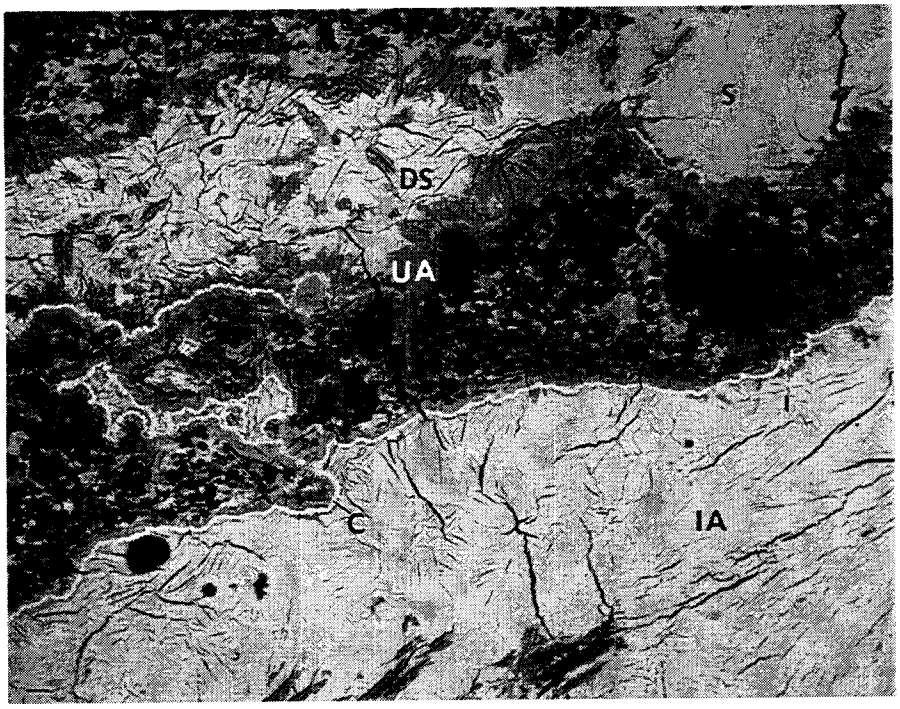

Figure 3-11. Backscattered electron photomicrograph of multiple uranium phases filling open space and replacing granular uraninite. Open space is filled by relatively coarse crystalline ianthinite (IA) followed by schoepite (S) and dehydrated schoepite (DS). Uranophane (UA) replaces all three uranyl oxide hydrates. Granular uraninite has been replaced by both schoepite and uranophane. Notice also the thin rim of colloform uraninite (C) that is preserved along the margins of the granular material in some areas. Field of view is 0.4 mm wide.

oxidizing fluids over long periods of time in an environment perceived to be pervasively oxidizing.

Schoepite (nominally $UO_3 \cdot 2H_2O$) is the most common uranyl oxide hydrate at Nopal I. In nature, schoepite exists as two polytypes (schoepite and meta-schoepite) that possess slightly different crystal structures (Finch and Ewing, 1992). The dehydration of schoepite proceeds directly to dehydrated schoepite $UO_3 \cdot 0.8H_2O$ (Finch and Ewing, 1992). Although the crystal structures of the schoepite minerals have not been totally resolved, it is clear that schoepite is the earlier phase and has the highest hydration state (Finch and Ewing, 1992).

At Nopal I, schoepite and/or dehydrated schoepite commonly fill open spaces that are lined by colloform uraninite (Figure 3-5). Both schoepite and dehydrated schoepite consist of relatively coarse (20 to 200 ,25 μm) equigranular to acicular crystals. Schoepite has also been tentatively identified in strongly oxidized rock centimeters away from uraninite-bearing areas, where it is either intergrown with uranyl silicates or forms radiating clusters of acicular crystals that appear to postdate uranyl silicate formation. As noted above, schoepite also forms by oxidation of ianthinite, both in the field and in the laboratory. In general, schoepite occurs as the fracture filling after uraninite and is generally followed or replaced by the uranyl silicates uranophane and soddyite (Figure 3-12).

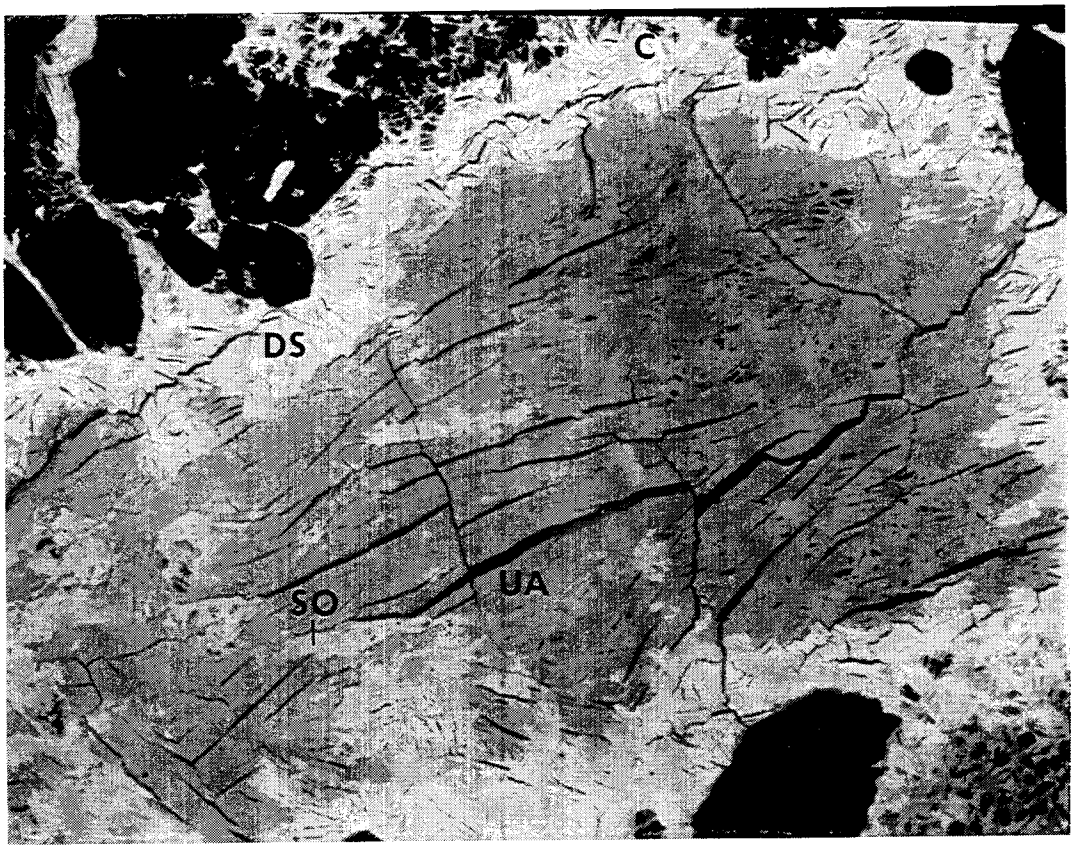

Figure 3-12. Backscattered electron photomicrograph of a fracture containing dehydrated schoepite (DS) at the margins followed by soddyite (SO) and uranophane (UA). A thin rim of colloform uraninite (C) is preserved along the top margin wall. Field of view is 400 microns wide.

Petrographically, schoepite can be identified by its brown to amber color under crossed nicols, whereas dehydrated schoepite is yellow. Additionally, there is a textural difference between schoepite and dehydrated schoepite at Nopal I, which is apparent with backscattered feel ectron imaging. The surface of schoepite is smooth, whereas microcracks are observed within dehydrated schoepite (Figure 3-11). These microcracks are caused by dehydration of precursor schoepite (Finch and Ewing, 1992).

Other minor uranyl oxide hydrates recognized at Nopal I are rich in barium or arsenic and potassium. The Ba-rich phase is tentatively identified as billietite [nominally $Ba(UO_2)_6O_4(OH)_6 \cdot 4$-$8H_2O$]. EMPA analyses, however, show only 2 to 3 weight percent Ba, suggesting some other unrecognized Ba phase, multiphase intergrowths, or an inaccurate measurement of the composition. This Ba-rich phase occurs in isolated microfractures within strongly oxidized ore, and appears to postdate the formation of other uranyl oxide hydrates. The As-K-rich phase is tentatively identified as abernathyite [nominally $K(UO_2)(AsO_4) \cdot 4H_2O$]. Again, however, EMPA analyses show less As and K (4 weight percent As and 2 weight percent K) than would be expected for stoichiometric abernathyite. The As-K-rich phase fills open space rimmed by colloform uraninite, and postdates the formation of other uranyl oxide hydrates (Figure 3-4). Becquerelite [nominally $Ca(UO_2)_6O_4(OH)_6 \cdot 8H_2O$], a calcium-rich uranyl oxide hydrate, has been identified by XRD analysis but has not been observed optically.

3.3 URANYL SILICATES

Uranyl silicates are the predominant uranium phases at Nopal I. Uranyl silicates occur as pseudomorphs of earlier formed uranium minerals and as euhedral crystals within voids and fractures. Whether uranyl silicates directly replace uraninite or replace uranyl oxide hydrates after uraninite is unclear. In specimens containing both uranyl silicates and uranyl oxide hydrates, evidence for the latter is observed. For example, in open voids lined by uraninite, a clear progression from uraninite to uranyl oxide hydrates to uranyl silicates is frequently preserved (Figure 3-12).

Soddyite [nominally $(UO_2)_2SiO_4 \cdot 2H_2O$] at Nopal I generally occurs within Fe-oxide rich fractures close to (within centimeters of) uraninite-bearing zones and typically follows uranyl oxide hydrate formation. In fractures lined with colloform uraninite, soddyite is observed filling void space with relatively large (30 to 50 μm) crystals (Figure 3-4). This soddyite is commonly associated with crystals of an As- and K-rich uranyl oxide hydrate, which has a similar abundance and crystal size. The presence of corroded uranyl oxide hydrates preserved in these voids suggests that soddyite replaces earlier uranyl oxide hydrates.

In portions of the deposit that are strongly oxidized, soddyite generally forms 5- to 20- μm, equant, yellow-orange crystals that are intergrown with other uranyl silicates including uranophane, weeksite, and boltwoodite (Figure 3-13). Euhedral rhombic soddyite crystals are often observed in late vugs and fractures along with kaolinite and/or smectite. These crystals are relatively coarse (50 to 100 μm) and have dipyramidal terminations. In some fractures, soddyite is juxtaposed with granular uraninite in a continuous and gradational manner, suggesting that the original uraninite was altered to pseudomorphs of soddyite by a bulk replacement of the primary mass. These soddyite crystals are anhedral and have maximum dimensions of about 5 μm, as did the precursor uraninite crystals. The kaolinite intergrown with the original uraninite remains intergrown with the replacement soddyite and appears to have been unaffected by the alteration of the uraninite to soddyite. Finally, within silicified, uraninite-bearing samples, veinlets up to 30 μm wide composed entirely of fine (< 10 μm) equigranular soddyite crosscut all earlier uranium mineralization, suggesting that at least a portion of the soddyite formed relatively late.

Uranophane [nominally $Ca(UO_2)_2Si_2O_7 \cdot 6H_2O$] is the most abundant secondary uranium mineral at Nopal I and occurs throughout the deposit. Its polymorph, beta-uranophane, is also present. X-ray diffraction analyses indicate that uranophane and beta-uranophane coexist in the center of the deposit, whereas the outer portions of the deposit contain predominantly uranophane.

Like soddyite, uranophane in some fractures is juxtaposed with granular uraninite in a continuous and gradational manner. Microprobe analyses and optical microscopy indicate that kaolinite is unaffected either compositionally or morphologically by the replacement of the uraninite by uranophane. Uranophane in vugs and fractures within or adjacent to uraninite-bearing breccia occurs as fine, equant, yellow to yellow-green crystals. Under backscattered electron imaging, uranophane displays microcracks similar to those observed in dehydrated schoepite (Figure 3-12). This feature may be a dehydration phenomenon or a replacement texture. In specimens containing both dehydrated schoepite and uranophane, uranophane is generally observed to have formed after the dehydrated schoepite suggesting the latter process.

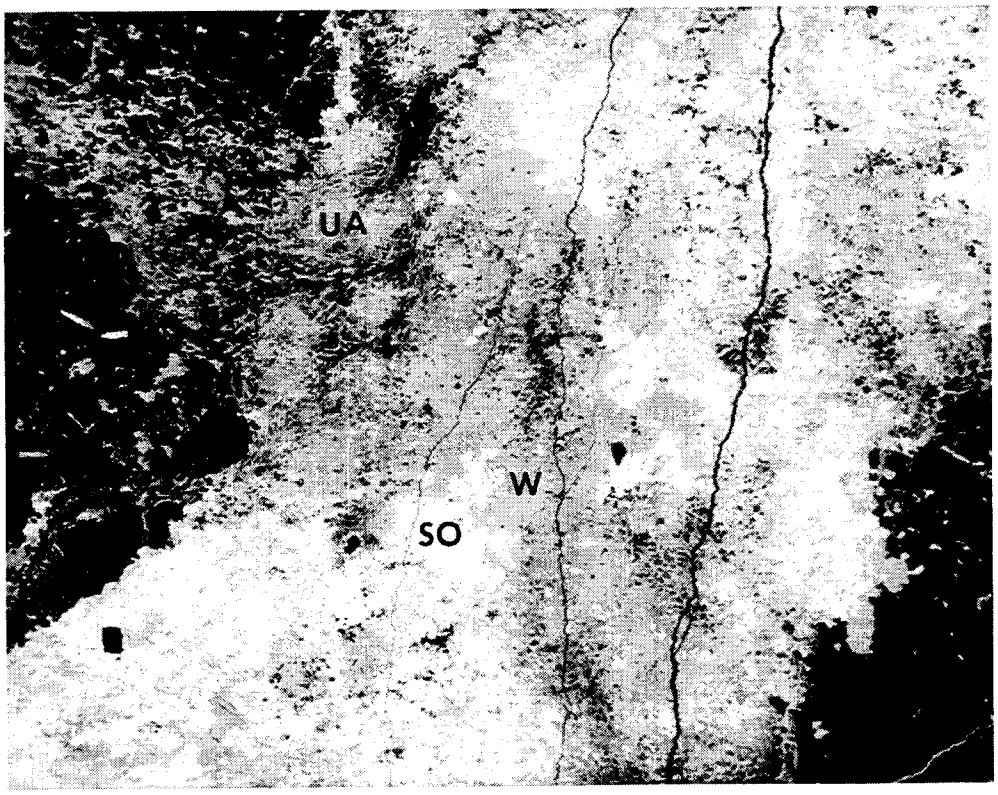

Figure 3-13. Backscattered electron photomicrograph of intergrown soddyite (SO), uranophane (UA), and weeksite (W) filling a fracture in a highly oxidized sample. Uranophane tends to occur along the fracture margins whereas weeksite tends to occupy the center of the fracture. Field of view is 1.1 mm wide.

In highly oxidized breccia containing multiple secondary uranium phases, uranophane tends to line fracture margins, suggesting that uranophane precipitated earlier than the other vein-filling uranium minerals (Figure 3-13). Throughout the orebody, open voids and fractures contain relatively coarse (100 μm to 3 mm) uranophane crystals. Alpha-uranophane in these voids and fractures generally forms clusters of yellow acicular crystals, whereas beta-uranophane precipitates as yellow-orange prismatic crystal masses. These well-formed crystals have often formed upon iron oxide substrates, indicating relatively late formation.

Weeksite [nominally $K_2(UO_2)_2Si_6O_{15} \cdot 4H_2O$] and boltwoodite [nominally $HK(UO_2)SiO_4 \cdot 1.5H_2O$] have much more restricted occurrences than uranophane. Remnant uraninite often occurs juxtaposed with uranophane and/or soddyite whereas weeksite and boltwoodite tend to occur somewhat further away (centimeters) from the uraninite. The similar habits, occurrence, composition, and structure of weeksite and boltwoodite make it difficult to differentiate optically between them in many cases. Weeksite and/or boltwoodite are composed of fine (<20 μm) equigranular, yellow anhedral crystals intergrown with uranophane and soddyite (Figure 3-13). In fractures containing multiple uranium phases, weeksite and boltwoodite tend to grow over earlier phases and to occupy the center of the veinlet, suggesting relatively late formation. In open fractures in the outer portion of the deposit, weeksite forms relatively coarse (20 to 200 μm) acicular radiating crystal masses.

3.4 PARAGENESIS OF URANIUM MINERALS AT NOPAL I

Primary uranium-bearing fluids at Nopal I originally deposited uranium in the form of uraninite. XRD and EMPA data suggest that this original uraninite may have contained more oxygen (approximately $UO_{2.2}$) than ideal uraninite (UO_2). Relations between uraninite textures and S and impurity cation concentrations suggest an alteration process in which primary uraninite was partially dissolved and reprecipitated in a different form. Texturally, euhedral and granular uraninite appear to have formed earlier than colloform uraninite. Euhedral and granular uraninite typically are intergrown with kaolinite and pyrite, whereas colloform uraninite is free of discernible primary intergrowths. All analyses of euhedral uraninite indicate a low sulfur content and enrichment in other cations. Except for one analysis of granular uraninite, all analyses with elevated S contents above 0.15 atom percent and low impurity cation contents are colloform in texture. Granular uraninites have compositions that tend to span the compositional range observed for the other textures.

These observations are consistent with an alteration scenario in which an acid sulfate solution generated by pyrite oxidation, containing potassium and silica, interacted with early-formed euhedral and granular uraninite. Portions of the euhedral and granular uraninite were dissolved, uranium may have been transported a short distance (millimeters to centimeters), and reprecipitated as colloform uraninite. This process leached Ca, Na, Pb and other cations from the uraninite, and precipitated colloform uraninite enriched in S and free of kaolinite and pyrite. This scenario is similar to inferences made for uraninite paragenesis at the Oklo uranium deposit at which uraninite containing V, Se, Mo, and Fe in low-grade ore is interpreted to have been dissolved and reprecipitated as high-grade (i.e., relatively pure) uraninite ore "effectively segregated from most of the elements associated with ... the low-grade ore" (Brookins, 1984).

The scenario invoked for the relatively pure colloform uraninite formation suggests that the microprobe analyses could be used to date the uraninite by the chemical Pb-U,Th method more robustly. These cation-free (i.e., low Ca/U and Pb/U) uraninites would better satisfy the constraints of negligible nonradiogenic lead, and the calculated dates would then more closely reflect the age of formation of the colloform uraninite. It should be noted that the only microprobe analyses that produce chemical Pb-U,Th dates less than the age of formation of the host rock formation are the cation-free uraninites. Using the seven low cation content colloform uraninite analyses (Table 3-3) and not correcting for common lead, an average age of formation of these uraninites is 7.9 $\pm$ 5.2 Ma (1 s). Errors quoted in Table 3-3 are based on the assumption of an average analytical error for Pb of 0.01 atom percent (the calculated date for samples less than 50 Ma is primarily dependent on Pb measurements). This calculation provides a maximum age of formation of the analyzed colloform uraninites (Hofmann and Eikenberg, 1991). Previous calculations based on microprobe analyses of low Ca/U and Pb/U uraninites, formed during a U remobilization event in the Swiss Alps, resulted in concordant uncorrected chemical U-Pb, U-Xe, and U-Kr ages (Eikenberg et al., 1989), lending some support to the above calculated uncorrected age of formation of the colloform uraninite.

Five analyses of euhedral uraninite (from a total of eight) taken from two samples all have similar U and corrected O contents of 27.52 $\pm$0.07 (1σ) and 60.58 $\pm$0.34 (1σ) atom percent, respectively, corresponding to a stoichiometric ratio of $UO_{2.20\ \pm 0.02(1\sigma)}$. One analysis of euhedral uraninite from a third sample has a corrected O/U ratio in this range. The primary nature of euhedral uraninite according to the postulated paragenetic scenario, the uniformity of the analyses, and the realistic stoichiometry suggests that these analyses provide an indication of the oxidation state of the primary uraninite mineralization.

Table 3-3. Electron microprobe U-Pb ages

Sample	U (atom %)	Pb (atom %)	Th (atom %)	Chemical Age (Ma)	±
32-ts2-p1	32.34	0.05	0.01	9.65	1.93
32-ts2-p4	30.88	0.04	0.00	8.09	2.01
32-ts2-p5	33.78	0.02	0.00	3.70	1.85
32-ts2-p6	32.79	0.07	0.02	13.31	1.90
1-ts3-p1	30.28	0.05	0.01	10.31	2.05
1-ts3-p2	30.09	0.02	0.01	4.15	2.07
1-ts3-p6	30.76	0.03	0.00	6.09	2.03

Subsequent to the limited, early dissolution and reprecipitation of Nopal I uraninite, the entire deposit underwent substantial alteration accompanied by uranium movement within and around the deposit and the formation of secondary uranium and nonuranium minerals. As exposed on the +10 m level of the Nopal I deposit, the center of the deposit is depleted in uranium and is enriched in K-Fe sulfate minerals (jarosite and alunite) relative to the periphery (Leslie et al., 1993). This apparent removal of uranium from the core of the deposit and formation there of sulfate minerals may have been caused by oxidizing, low pH fluids produced by oxidation of primary pyrite within the deposit.

Uraninite has been oxidized and has reacted with aqueous solutions containing alkalis, alkaline earths, and silica as well as various trace constituents (e.g., As and Ti), producing an ordered suite of secondary uranyl oxide and uranyl silicate minerals (Figure 3-14).

The initial minerals formed by uraninite alteration at Nopal I are uranyl oxide hydrates that directly replace uraninite and fill voids lined by uraninite. In samples containing multiple uranyl oxide phases, ianthinite is the earliest formed uranyl oxide hydrate and is followed by schoepite and/or dehydrated schoepite. Schoepite is frequently intergrown with uranyl silicates (e.g., uranophane, weeksite, boltwoodite, and soddyite).

Uranyl oxide hydrates are contemporaneous with and are followed paragenetically by uranyl silicates. Uranyl silicates juxtaposed with granular uraninite frequently occur as pseudomorphs after the primary uraninite. It is likely that this replacement is a two-stage process in which the uraninite is first altered to uranyl oxide hydrates, which are then altered to uranyl silicates. In samples that contain all three phase types, evidence for a clear progression from uraninite to uranyl oxide hydrates to uranyl silicates is sometimes preserved. In other cases, schoepite grows over uranophane.

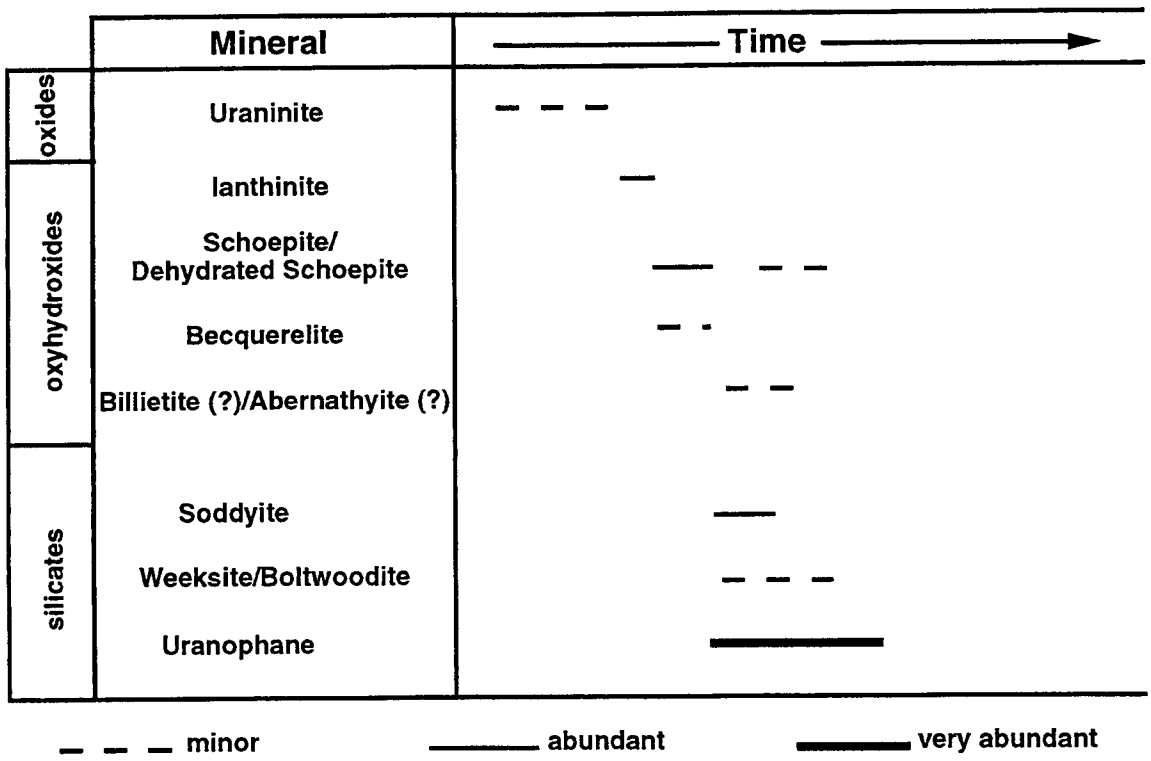

Figure 3-14. Relative sequence of formation and abundance of uranium minerals at the Nopal I deposit.

Specifically, in the most reduced samples from Nopal I (i.e., those containing uraninite), soddyite and uranophane are juxtaposed with granular uraninite in a continuous and gradational manner, suggesting that the original uraninite was altered to pseudomorphs composed of these uranyl silicates by a bulk replacement of the primary mass. In vugs and fractures in reduced samples, uranophane and soddyite are observed overgrowing dehydrated schoepite. Also within uraninite-bearing samples, veinlets of soddyite crosscut all earlier uranium mineralization, suggesting that at least some soddyite formed relatively late.

In strongly oxidized samples, uranophane tends to line fracture margins and is itself intergrown with other uranyl silicate phases, including soddyite, weeksite, and boltwoodite. The occurrence of weeksite and boltwoodite somewhat further from remnant uraninite than uranophane and soddyite may indicate their formation later in the sequence; this late formation is supported by the presence of weeksite and boltwoodite as late overgrowths covering earlier uranyl silicates. Coarse, euhedral uranophane growing upon iron oxide substrates in voids and fractures also indicates a relatively late formation.

Typically, uranyl silicate minerals occur intimately intergrown with each other. Samples that show a clear progression from one uranyl silicate to another must be reconciled with other samples that show a different sequence. This evidence, taken together with that above, suggests that, at Nopal I, uranyl silicates generally formed after uranyl oxide hydrates, but that the specific uranyl silicate formed

in a given area depended on the local geochemical conditions rather than on broad evolution of the oxidizing system. Such local variability is characteristic of natural systems.

4 DISCUSSION

The oxidative alteration of uraninite in the Nopal I system may be similar to the oxidative alteration of spent nuclear fuel that would occur if emplaced in a HLW repository within Yucca Mountain. As described earlier, the present geologic environment of the Nopal I deposit resembles closely that of the proposed HLW repository at Yucca Mountain, Nevada. Nevertheless, there are differences between the two systems. Comparisons between the geologic environments of Nopal I and Yucca Mountain and between natural uraninite and spent nuclear fuel are useful to clarify the potential and the limitations of the analog.

4.1 MINERALOGIC COMPARISON OF NOPAL I URANINITE AND SPENT FUEL

The occurrence and persistence of uraninite in the Nopal I system is both unusual geochemically and fortuitous as a comparison to a Yucca Mountain HLW repository. In most hydrologically unsaturated, chemically oxidizing deposits, uranium exists as U^{+6} and occurs as uranyl (UO_2^{2+}) species in various minerals. Nopal I is remarkable in that some of the original uraninite remains so that the alteration sequence may be examined in its entirety.

Natural uraninite is a close structural and compositional analog to spent nuclear fuel. Spent fuel, like uraninite, is greater than 95 percent UO_2 (Barner, 1985). Spent fuel and uraninite have the same cubic crystal structure [fluorite type, space group *Fm3m* (Frondel, 1958)], and both are subject to radiation damage to the crystal lattice. There are, however, some significant differences between spent fuel and natural uraninite. Spent fuel, depending on the operating conditions of the reactor and the degree of burnup, is subject to considerable structural damage during irradiation, whereas natural uraninite sustains damage principally in the form of atomic displacements caused by spontaneous alpha decay and nuclear recoil (Finch and Ewing, 1990). Such damage may affect the dissolution behavior of the damaged areas of the crystal (Fleischer, 1988), but the long-term effects of radiation damage on the structure of uraninite are poorly understood (Finch and Ewing, 1990). The effects on fuel are even less well understood.

Prior to irradiation, nuclear fuel has a stoichiometry close to UO_2. Oxygen is produced during irradiation but is almost quantitatively removed from the fuel by diffusion at the elevated operating temperatures of the reactors; the removed oxygen combines with the zircaloy cladding around the fuel and is effectively prevented from further interaction with the fuel (Kleykamp, 1979). As a result, the irradiated fuel has a final stoichiometry again close to UO_2 (Kleykamp, 1979). This is a more reduced starting condition than that inferred for Nopal I uraninite, which appears to have formed initially with an O/U ratio close to 2.2.

Natural uraninite typically contains a variety of trace elements in solid solution within the crystal structure. As discussed earlier, uraninite from the Nopal I deposit appears to contain significant Ca, Si, K, Pb, Na, and Al. Uraninite from other localities commonly contains substantial Fe, Th, and rare earth elements in addition to those elements present at Nopal I (Frondel, 1958). Electron microprobe analyses indicate that, on average, trace elements comprise about 3 weight percent of Nopal I uraninite. Similarly, spent fuel contains many impurities, most of which are produced during irradiation (e.g., Pu, Mo, Sr, Ba, Cs, and many others) (Findlay, 1972a; Johnson and Shoesmith, 1988; Woodley, 1983). Though the amounts of these trace constituents vary with the degree of burnup of the fuel and time since irradiation,

impurities generally comprise less than 5 weight percent of discharged fuel (Barner, 1985). It should be noted that the identities of the trace elements in spent fuel are different from those in Nopal uraninite. A further difference between spent fuel and Nopal uraninite is that, in addition to impurities contained within the crystal structure, spent fuel typically contains discrete phases composed of fission products that migrate through the UO_2 lattice. These fission products tend to form separate phases concentrated along grain boundaries (Findlay, 1972b; Kleykamp, 1972; Kleykamp, 1985); such phases are absent from Nopal uraninite.

In summary, uraninite from the Nopal I deposit compares closely to spent nuclear fuel in terms of bulk composition, crystal structure, total trace element content, and oxidation state (U/O ratio). There are significant differences between Nopal I uraninite and spent nuclear fuel with regard to degree of radiation damage, trace element identities, and the presence of discrete phases along grain boundaries. Detailed characterization of these differences and their significance is the subject of continuing research.

4.2 COMPARISONS TO LABORATORY EXPERIMENTS

The mechanisms of alteration of uraninite at Nopal I and the nature and sequence of the resulting secondary phases may be compared to the results of oxidation experiments conducted using unirradiated UO_2 or spent fuel. Such comparisons allow evaluation of the degree to which laboratory experiments, which are necessarily relatively brief (e.g., 1 to 10 years maximum duration), reflect the long-term behavior at Nopal I. Differences in alteration mechanisms may be due to disparities between the Nopal I system and the experiments. Similarities may indicate insensitivity of the alteration mechanisms to the differences.

The small crystal size of the uraninite (5 to 10 μm) at Nopal I presents a large reactive surface area and results in pervasive replacement of the bulk uraninite as it reacts with oxidizing fluids. In the Nopal I system, the oxidation of the uraninite is a result of both fluid flow along uraninite-bearing fractures and fluid movement through the matrix of breccia fragments. In fractures, alteration typically produces an approximately symmetric change in the mineralization, with relatively unaltered uraninite remaining along the margins of the vein and the center of the vein filled with secondary uranyl minerals. The reaction front generally has an arcuate form, with the most advanced zone located near the center of the vein, recording reduced fluid flow and/or chemical reaction near the fracture margin. This style of alteration produces a diffuse reaction front, with a gradual transition from unaltered uraninite to uraninite completely replaced by uranyl minerals occurring over a distance of about 100 μm. Frequently, the outermost edges of oxidation fronts (whether along veinlets or within breccia fragments) have an iron oxide halo (about 150 μm wide). This halo suggests that the altering fluids oxidized iron present in pyrite within the primary mineral assemblage.

This pattern of alteration of the bulk assemblage of the fine-grained uraninite at Nopal I is similar to alteration of unirradiated UO_2 and spent fuel in laboratory experiments. The crystal size and form of Nopal I uraninite (5- to 10- μm equant grains) is close to that of spent fuel [6- to 25- μm equant grains (Wilson, 1990a)], and it is reasonable to compare the patterns of advance of oxidation fronts. There are few reports of the form of such alteration fronts observed in laboratory experiments where spent fuel has been exposed to oxidizing aqueous solutions. In an investigation of spent fuel oxidation in air (Thomas et al., 1991), it was found that oxidation preferentially advanced along grain boundaries with complete oxidation of individual UO_2 grains only after passage of the leading edge of the oxidation front. Much deeper penetration of the oxidation front occurred along the original fuel pellet rim than along preoxidation fracture surfaces. The alteration horizon was irregular in form, with deeper

penetration perhaps related to areas of increased porosity in the fuel, though the correlation of enhanced oxidation with areas of increased porosity was not consistent.

There are differences in the patterns of oxidation of spent fuel and unirradiated UO_2 (Einziger et al., 1992). Whereas spent fuel preferentially alters initially along grain boundaries, laboratory alteration of unirradiated UO_2 typically begins with formation of a thin layer (e.g., up to a few μm depth) of oxidized uranium phases on the surface of the UO_2 (e.g., Shoesmith et al., 1989; Sunder et al., 1991). Some experiments have reported a tendency for grain boundary oxidation of unirradiated UO_2 (Taylor et al., 1980). In general, preferential oxidation along grain boundaries in unirradiated UO_2 proceeds only a short distance into the UO_2 (e.g., some tens of μm); in contrast, grain boundary oxidation in spent fuel may extend well into the fuel. There is also a tendency for oxidation of unirradiated UO_2 to form U_3O_7 rather than U_4O_9 as does spent fuel (Einziger et al., 1992).

The oxidation fronts observed in spent fuel tests and in the oxidation of unirradiated UO_2 may correspond to the leading edge of the alteration front observed on the Nopal I uraninite in which the uraninite passes through a transition zone to uranyl phases. X-ray diffractometry and calculations of the residual oxygen content of the least altered Nopal I uraninite suggest that it may have originally formed as $UO_{2.23}$ to $UO_{2.25}$. Thus, the uraninite began as a phase close to U_4O_9, precluding observation of initial grain boundary alteration from UO_2 to U_4O_9 as observed in laboratory experiments. Alteration of the primary Nopal I uraninite to uranyl phases occurs over a broader zone than is typical for unirradiated UO_2 oxidized in air. The penetrative oxidation of the Nopal I uraninite compares more closely to the general patterns observed for spent fuel degradation. However, as noted, Nopal I uraninite does not exhibit clear grain boundary alteration as does spent fuel.

One of the most significant differences between the oxidation of Nopal I uraninite and that of spent fuel or unirradiated UO_2 is the much shorter duration of the laboratory experiments compared to the time since formation of the Nopal I uraninite (e.g., 10^6 years). The depth of penetration of the oxidation front into natural uraninite masses at Nopal I (up to centimeters) may be interpreted as comparable to the scales anticipated for oxidation of spent fuel over long time periods. It may be expected, therefore, that fuel pellets [cylinders with nominal dimensions of about 8 mm diameter and 10 mm length (Manaktala et al., 1991)] would become completely oxidized (i.e., to uranyl minerals) over long time periods during storage under conditions likely to be present in a Yucca Mountain repository.

As described above, the sequence of secondary minerals formed during oxidation of uraninite in the Nopal I system is likely to be similar to that which would occur over long time periods in a Yucca Mountain repository, after exposure of the spent fuel to the ambient geochemical environment. Comparison of the sequence of uraninite alteration products formed at Nopal I to those formed during laboratory experiments designed to investigate the oxidation of spent fuel or unirradiated UO_2 in a Yucca Mountain environment is instructive.

In a series of experiments (Wilson, 1990a; Wilson, 1990b; Wilson, 1991; Wilson and Bruton, 1989), spent fuel was reacted with water from the J-13 well at Yucca Mountain. J-13 water is collected from the hydrologically saturated zone of Yucca Mountain from rocks corresponding stratigraphically to the proposed repository horizon. The J-13 water has often been used to approximate fluids in the unsaturated zone. Samples of fuel from the H. B. Robinson Unit 2 (the ATM-101 material described in Barner, 1985) and the Turkey Point Unit 3 pressurized water reactors were submerged in J-13 water (Table 4-1) in unsealed silica reaction vessels at 25°C for 34 months (Series 2) and in sealed stainless steel reaction vessels at 25°C and at 85°C for 15 months (Series 3). Study of the alteration products was

Table 4-1. Compositions of Altering Fluids (concentrations in mg/ml)

	pH	Al	PO_4	Cl	F	NO_3	SO_4	B	CO_3	Ca	Mg	K	Na	Si
J-13	7.2	0.11	2.8	7.3	2.7	8.7	18.8	<0.10	118.0	15.0	2.1	5.5	49.5	31.9
EJ-13	8.2	na	na	8.6	2.8	8.2	21	0.16	18.4[a]	9.08	0.96	8.08	46.5	34.4
BH12	7.5	0.17	na	3.0	1.6	2.5	39	na	161.5[b]	57.7	<1.0	1.5	13.8	37.9

J-13 data from Wilson, (1990a). EJ-13 data from Wronkiewicz et al., (1992). BH12 data from Pearcy et al., (1991).

[a] For EJ-13, total inorganic carbon, as reported
[b] For BH12, HCO_3, as reported
na = not analyzed

not a major focus of these investigations, but brief descriptions were provided of uranium alteration minerals discovered on filters used during the tests.

The Series 2 tests found only one secondary uranium mineral, tentatively identified as haiweeite [$Ca(UO_2)_2Si_6O_{15} \cdot 5H_2O$]. The Series 3 tests identified uranophane, haiweeite, and possible soddyite. Uranophane had an acicular, radiating habit, whereas the haiweeite had a "flake-like" morphology. Soddyite morphology was not reported. The relative abundances of uranyl silicate minerals formed during the Series 3 tests parallel those observed at Nopal I with uranophane as the most common, followed by lesser amounts of soddyite. Haiweeite, however, has not been identified at Nopal I. Its absence may reflect differences in the compositions of the altering fluids, temperatures, or kinetics of the driving reactions.

In another set of experiments (Bates et al., 1990; Wronkiewicz et al., 1992), unirradiated UO_2 was reacted at 90°C with J-13 water that had been "equilibrated" with rock from the proposed repository horizon at Yucca Mountain (Topopah Spring Tuff). EJ-13 water (Table 4-1) is significantly different from the unequilibrated J-13 water used in the saturated tests described previously. In particular, EJ-13 water has less Ca and Mg and more K than the J-13 water. These experiments continued for up to 4.5 years under unsaturated conditions. The equilibrated J-13 (EJ-13) water was periodically dripped onto the UO_2 in an attempt to simulate conditions likely to occur in a Yucca Mountain repository. The reaction products observed in these experiments conform closely to the secondary phase assemblages and sequences at Nopal I.

Wronkiewicz et al. (1992) found that secondary crystals from shorter term experiments (e.g., 78 weeks) had a single morphology, whereas long-term samples (up to 238 weeks) had several precipitate types. Preferential dissolution along grain boundaries during the long-term experiments was so advanced as to nearly detach UO_2 grains from the altered surfaces. There was a tendency for secondary phases to form a "mat" of corrosion products on the surface of the UO_2. This mat appeared to hold grains of UO_2 loosened by dissolution in place, but did not appear to protect the underlying surface from additional oxidation.

The general sequence of formation of the secondary uranium minerals in the experiments reported by Wronkiewicz et al. (1992) compares closely with the sequence observed at Nopal I:

- uraninite
- U oxide hydrates (e.g., dehydrated schoepite)
- soddyite
- U alkali silicates (e.g., uranophane followed by boltwoodite)

The detailed observations upon which this sequence is based also correspond well to patterns observed at Nopal I. For example, Wronkiewicz et al. (1992) observed that soddyite replaced schoepite in some places, whereas in other places, soddyite formed directly on the UO_2 surface. The absence of schoepite on samples terminated after 2.5 years was interpreted by Wronkiewicz et al. (1992) to indicate replacement of schoepite by more stable assemblages composed of silicates. Similarly, at Nopal I, soddyite is observed both as a replacement of schoepite and in direct contact with uraninite with no intermediate phases. Schoepite, however, is observed to follow uraninite directly in some samples but is never observed to replace soddyite. At both Nopal I and in the experiments of Wronkiewicz et al. (1992), complex intergrowths of secondary minerals occur and are interpreted to indicate simultaneous precipitation of those phases (Wronkiewicz et al., 1992).

Of course, the conditions under which uraninite oxidized at Nopal I were different in many aspects from those used in the unirradiated UO_2 and spent fuel oxidation experiments described above. Those differences are responsible, in part, for variations in secondary uranium mineral occurrence within the respective systems. Differences between the secondary mineral assemblages identified experimentally and those observed at Nopal I are reasonably small, considering the experimental studies of Wronkiewicz et al. (1992) were conducted with no emphasis on the natural system at Peña Blanca. Of particular significance is the occurrence of some secondary phases in the experiments that are not observed in the Nopal system. In addition to the minerals listed above, Wronkiewicz et al. (1992) identified extremely rare occurrences of sklodowskite [$(H_3O)2Mg(UO_2)_2(SiO_4)_2 \cdot 2H_2O$] and possible occurrences of compreignacite [$K_2(UO_2)_6O_4(OH)_6 \cdot 8H_2O$] in their experimental sequences. Neither sklodowskite or compreignacite has been identified as part of the alteration sequence at Nopal I. The experimental apparatus used by Wronkiewicz et al. included stainless steel reaction vessels that may have contributed to the formation of Fe-oxides, Ti-Si-Fe-Al, Mg-Si-Fe, and Al-Si-Ni precipitates on and around the UO_2 test samples. These nonuranium phases have some parallels in the Nopal I system (e.g., abundant Fe-oxides associated with the uranium mineralization), but, in general, the comparisons among nonuranium phases in the two systems are not close.

It is not certain if uraninite oxidation at Nopal I is a product only of episodic infiltration of the deposit by meteoric fluids or was caused by post ore-formation hydrothermal fluids passing through the deposit or some combination of these processes. Alteration of uraninite to the present suite of secondary uranium minerals may have occurred as a result of more than one event and may have spanned considerable time (e.g., 10^5 to 10^6 years). Nevertheless, it is apparent from the compositions of the secondary phases at Nopal I that the altering fluids were oxidizing and contained substantial silica, calcium, and potassium. This composition probably reflects interaction of the altering fluids with the host tuffs, which have abundant silica (largely as glass shards) and significant amounts of calcium (0.4 to 4.4 weight percent) and potassium (4.1 to 6.5 weight percent). Additional calcium (as reflected in the abundance of uranophane in the system) may also have been supplied by limestones that underlie the volcanic sequence or by interaction of descending meteoric fluids with caliche near the surface (Murphy et al., 1991) and/or with abundant calcite veinlets in the deposit area.

Recently (i.e., since tilting and uplift of the Basin and Range horst, which is the structural host block for the Nopal I deposit), the most likely mechanism for introduction of oxidizing fluids to alter the remaining uraninite at Nopal I is episodic penetration of the host tuffs by meteoric water. An estimate of the composition of these fluids is provided by analyses of rainwater trapped in a 10- m deep vertical drillhole located about 20 m from the perimeter of the deposit (BH12, Table 4-1). This water accumulated in the drillhole during a series of rainstorms and was allowed to react with the tuff, open to the atmosphere, for a period of about 3 weeks prior to sampling. BH12 had been open to episodic infiltration for a period of about 10 years.

The BH12 water is similar to J-13 and to EJ-13 with respect to pH, silica, F, and Mg concentrations. Nevertheless, BH12 water has higher Ca (57.7 ppm) and SO_4 (39 ppm) than either J-13 (15.0 and 18.8 ppm, respectively) or EJ-13 (9.08 and 21 ppm, respectively). Conversely, BH12 has significantly lower Cl (3.0 ppm), K (1.5 ppm), and Na (13.8 ppm) than J-13 (7.3, 5.5, and 49.5 ppm, respectively) and EJ-13 (8.6, 8.08, and 46.5 ppm, respectively).

These disparities are significant and may be the cause of differences between the secondary mineralization of the Nopal I deposit and the experimental systems. The relatively high BH12 Ca concentration may be a product of interaction of the rainwater with surface and near-surface caliche

and/or earlier formed calcite veinlet linings also present in the deposit area. This Ca abundance is consistent with the dominance of uranophane among the uraninite oxidation products at the site and with the spatial distribution of uranophane. Uranophane is widely distributed throughout the deposit, suggesting a considerable mass and activity of Ca through most of the system. However, soddyite (the cation-free uranyl silicate) and weeksite (the main K-uranyl silicate) have a much more limited occurrence and are generally restricted to the center of the deposit (Ildefonse et al., 1990b). Ca is also likely to be an important control on secondary phases formed after spent fuel oxidation in a Yucca Mountain repository. As at Nopal I, the Yucca Mountain area has abundant Ca available in the form of caliches and calcite-filled veinlets near the surface, and as carbonate sedimentary rock present below the tuffs. Consequently, uranophane is likely to dominate the secondary phases formed upon long-term exposure of spent fuel to the Yucca Mountain geochemical environment (Murphy et al., 1991).

The substantial SO_4 values in the BH12 water may derive from oxidation of sulfide minerals present as part of the primary Nopal I mineralization or dissolution of sulfates formed during intermediate alteration of the Nopal I system. Such reactions could produce acids promoting dissolution of uraninite, calcite, or silicates. The BH12 fluids may be more representative of bulk solution compositions responsible for most of the Nopal I uraninite alteration in which the pH of the relatively small amounts of infiltrating fluids are broadly buffered by reaction with the volcanic host rock. Similarly, portions of the Yucca Mountain system may develop anomalously low pH values due to local mineral reactions or radiolysis from the spent fuel itself or reaction with some other engineered portion of the repository system. It is likely, however, that low pH solutions would not persist because of general buffering by the host tuffs and fluids to near neutral or slightly alkaline values comparable to BH12.

The Nopal I deposit contains some volumes in which bulk U concentrations are low, uranium mineralization is absent, and sulfate minerals (e.g., alunite and jarosite) occur (Leslie et al., 1992). Such occurrences are consistent with the hypothesis of locally acidic conditions within a broadly near-neutral system. The localized occurrence of sulfate minerals is consistent with the spatial variations in the composition of coeval uranyl silicates described above. In addition to spatial variations in system conditions, temporal variations in local conditions have likely occurred over the long period of alteration of the Nopal I system (e.g., 10^6 years). This sort of variation is characteristic of natural systems that are large relative to laboratory experiments and reflects heterogeneities in local conditions and availabilities of components. Such variations would not, however, be expected within the relatively small and homogeneous confines of a laboratory experiment.

5 CONCLUSIONS

Uraninite from the Nopal I deposit is a particularly good natural analog to spent nuclear fuel. In addition to attributes shared with uraninite from other deposits (e.g., cubic crystal structure and a bulk chemistry approximated by UO_{2+x}), Nopal I uraninite has a low total trace element component (average about 3 weight percent) that compares well with spent fuel, which typically has less than 5 weight percent trace constituents (Barner, 1985).

The compositions of secondary phase assemblages formed after alteration of uraninite depend on the available elements. In many uraninite deposits, the secondary uranium mineralogy is dominated by Pb or P minerals. Pb forms in uraninite by radiogenic decay over long time periods (e.g., 10^9 years), and considerable P is available in the ambient geochemical environment of some deposits. Neither of these elements is a major constituent of minerals in the Nopal I or Yucca Mountain systems. Pb, P, and V are present only in low concentrations in spent nuclear fuel [e.g., less than 10^{-8} weight percent, (Barner, 1985)] and are also present only in low concentrations in the Yucca Mountain environment [U.S. Department of Energy (DOE), 1988]. Therefore, Pb, P, and V minerals are unlikely to be formed as a result of spent fuel alteration at Yucca Mountain.

The most common trace element (on an atom fraction basis) in Nopal I uraninite is Ca (Table 3-2). Ca is also a common element in the local environment of the Nopal I deposit (e.g., carbonate rocks below the deposit, caliches and calcite veins above and at the elevation of the deposit). Consistent with this Ca abundance, the dominant secondary uranium phase at Nopal I is uranophane (a calcium uranyl silicate). Long-term laboratory experiments in which UO_2 was reacted with fluids containing Ca have produced uranophane as a common secondary phase (Wronkiewicz et al., 1992). Ca is also a common element in the environment of the proposed HLW repository at Yucca Mountain (carbonate rocks below the proposed repository horizon, caliches above and calcite veins around the proposed repository horizon). Ca-rich groundwaters are likely to be important in alteration of spent fuel in a Yucca Mountain repository. Under these conditions, uranophane is likely to dominate the secondary phase assemblages formed by long-term exposure of spent fuel to the Yucca Mountain geochemical environment.

Formation of specific uranyl mineral assemblages in a given portion of the Nopal I deposit depended on the local chemical environment rather than on broad evolution of the oxidizing system. The Nopal I system appears to have developed substantial local variations (on a scale of meters) in cation concentrations and pH during oxidation. Local chemical variability is characteristic of natural systems and will likely be present in a HLW repository.

There is substantial similarity between the results of laboratory experiments designed to study alteration of unirradiated UO_2 and spent fuel under simulated Yucca Mountain conditions and the alteration of natural uraninite at the Nopal I deposit. These similarities include the irregular, somewhat diffuse pattern of advance of the oxidation front through the UO_2/spent fuel/uraninite and the sequence of alteration products formed. The similarities in oxidation patterns suggest that the depth of penetration of the oxidation front into uraninite at Nopal I (up to centimeters) may be comparable to the oxidation of spent fuel over long time periods. Therefore, it may be expected that fuel pellets [cylinders with nominal dimensions of about 8 mm diameter and 10 mm length, (Manaktala et al., 1991)] would become completely oxidized (i.e., altered to uranyl minerals) over long time periods during storage under conditions likely to be present in a Yucca Mountain repository.

In laboratory experiments with unirradiated UO_2 and spent fuel and in natural oxidation of uraninite, there is a general trend from mixed uranium oxides, to uranyl oxyhydroxides, and finally to uranium silicates. Specifically, the end products of laboratory experiments designed to approximate Yucca Mountain conditions and the natural alteration of Nopal I uraninite in an environment analogous in many respects to Yucca Mountain are dominated by uranophane with lesser amounts of soddyite. The longest term laboratory experiments (4.5 years) developed alteration parageneses, intergrowths, and morphologies remarkably similar to those observed at Nopal I. These similarities in reaction product occurrence developed despite the differences in time and the physical-chemical environment between the laboratory experiments and uraninite alteration at Nopal I, suggesting that the likely range of spent fuel alteration phases is relatively limited. The close agreement developed under a range of conditions approximating conditions tenable for a Yucca Mountain repository suggests that the results may reasonably represent phases likely to form during long-term alteration of spent fuel in a Yucca Mountain repository.

6 REFERENCES

Airey, P.L. 1986. Radionuclide migration around uranium ore bodies in the Alligator Rivers region of the Northern Territory of Australia: analogue of radioactive waste repositories - a review. *Chemical Geology* 55:255-268.

Alba, L.A. and R. Chavez. 1974. K-Ar ages of volcanic rocks from the central Sierra Peña Blanca, Chihuahua, Mexico. *Isochron West* 10:21-23.

Barner, J.O. 1985. *Characterization of LWR spent fuel MCC-Approved testing material - ATM-101*. PNL-5109 Rev.1 UC-70. Battelle Pacific Northwest Laboratory.

Bates, J.K., B.S. Tani, E. Veleckis, and D.J. Wronkiewicz. 1990. Identification of secondary phases formed during unsaturated reaction of UO_2 with EJ-13 water. V. M. Oversby and P. W. Brown, eds. *Scientific Basis for Nuclear Waste Management XIII*. Pittsburgh: Materials Research Society: 499-506.

Brookins, D.G. 1984. Natural analogs. *Geochemical Aspects of Radioactive Waste Disposal*. New York: Springer-Verlag: 197-231.

Calas, G. 1977. Les Phenomenes d'Alteration Hydrothermale et leur Relation avec les Mineralisations Uraniferes en Milieu Volcnique: le cas des Ignimbrites Tertiaires de la Sierra de Peña Blanca, Chihuahua (Mexique). *Sciences Geologiques Bulletin* 30:3-18.

Cardenas-Flores, D. 1985. Volcanic stratigraphy and U-Mo mineralization of the Sierra de Peña Blanca District, Chihuahua, Mexico. *Uranium Deposits in Volcanic Rocks*. Austria: International Atomic Energy Agency, proceedings of a technical committee meeting, El Paso, TX April 1984. IAEA-TC-490: 125-136.

Cramer, J.J. 1986. Sandstone-hosted uranium deposits in northern Saskatchewan as natural analogs to nuclear fuel waste disposal vaults. *Chemical Geology* 55:269-279.

Curtis, D.B., T.M. Benjamin, and A.J. Gancarz. 1981. The Oklo reactors: natural analogs to nuclear waste repositories. P. L. Hofman, ed. *The technology of high-level nuclear waste disposal DOE/TIC-4621*. DOE: 255-283.

DOE. 1988. *Site characterization plan - Yucca Mountain site, Nevada Research and Development Area, Nevada*. DOE/RW-0199. DOE.

Eikenberg, J., V. Koppel, T. Labhart, and P. Signer. 1989. U-Pb, U-Xe and U-Kr systematics of a greenschist facies metamorphic uranium mineralization of the Siviez-Mischabel nappe (Valais, Switzerland). *Schweizerische Mineralogische und Petrographische Mitteilungen*. 69:331-344.

Einziger, R.E., L.E. Thomas, H.C. Buchanan, and R.B. Stout. 1992. Oxidation of spent fuel in air at 175 to 795°C. *Journal of Nuclear Materials* 190:53-60.

Finch, R.J. and R.C. Ewing. 1989. *Alteration of natural UO2 under oxidizing conditions from Shinkolobwe, Katanga, Zaire: a natural analogue for the corrosion of spent fuel.* Technical Report 89-37. Stockholm: Swedish Nuclear Fuel and Waste Management Company (SKB).

Finch, R.J. and R.C. Ewing. 1990. *Uraninite alteration in an oxidizing environment and its relevance to the disposal of spent nuclear fuel.* Technical Report 91-15. Stockholm: Swedish Nuclear Fuel and Waste Management Company (SKB).

Finch, R.J. and R.C. Ewing. 1991. Alteration of natural UO_2 under oxidizing conditions from Shinkolobwe, Katanga, Zaire: a natural analogue for the corrosion of spent fuel. *Radiochimica Acta* 52/53:395-401.

Finch, R.J. and R.C. Ewing. 1992. *Uranyl oxide hydrates and uraninite corrosion: relevance to "natural analogue: studies of spent fuel corrosion.* Third Annual International High-Level Radioactive Waste Management Conference. Las Vegas, Nevada: American Nuclear Society, Inc. and the American Society of Civil Engineers: 332-336.

Findlay, J.R. 1972a. The composition and chemical state of irradiated oxide reactor fuel material. *Behavior and Chemical State of Irradiated Fuels, Proceedings of Panel, Vienna.* Vienna: International Atomic Energy Agency, STI/PUB/303: 31-39.

Findlay, J.R. 1972b. The migration of fission products through reactor fuel materials. ed. *Behavior and Chemical State of Irradiated Fuels, Proceedings of Panel, Vienna.* Vienna: International Atomic Energy Agency, STI/PUB/303: 211-220.

Fleischer, M. 1988. Alpha-recoil damage: relation to isotopic disequilibrium and leaching of radionuclides. *Geochimica et Cosmochimica Acta* 52:1459-1466.

Frondel, C. 1956. Mineral composition of gummite. *The American Mineralogist* 41:539-568.

Frondel, C. 1958. *Systematic Mineralogy of Uranium and Thorium.* Geological Survey Bulletin 1064. Washington, D.C.: USGS.

Gauthier-Lafaye, F. and F. Weber. 1989. The Francevillian (Lower Proterozoic) uranium ore deposits of Gabon. *Economic Geology* 84:2267-2285.

George-Aniel, B., J.L. Leroy, and B. Poty. 1985. Uranium deposits of the Sierra Peña Blanca. *Uranium Deposits in Volcanic Rocks.* Austria: International Atomic Energy Agency, proceedings of a technical committee meeting, El Paso, TX April 1984. IAEA-TC-490: 175-186.

George-Aniel, B., J.L. Leroy, and B. Poty. 1991. Volcanogenic uranium mineralization in the Sierra Peña Blanca District, Chihuahua, Mexico: three genetic models. *Economic Geology* 86:233-248.

Goodell, P.C. 1981. Geology of the Pena Blanca uranium deposits, Chihuahua, Mexico. P. C. Goodell and A. C. Waters, ed. *Uranium in Volcanic and Volcaniclastic Rocks- AAPG Studies in Geology No. 13.* El Paso, TX: American Association of Petroleum Geologists: 275-291.

Hofmann, B. and J. Eikenberg. 1991. The Krunkelbach uranium deposit, Schwarzwald, Germany: Correlation of radiometric ages (U-Pb, U-Xe-Kr, K-Ar, ^{230}Th-^{234}U) with mineralogical stages and fluid inclusions. *Economic Geology* 86:1031-1049.

Ildefonse, P., P. Agrinier, and J.-P. Muller. 1990a. *Crystal chemistry and isotope geochemistry of alteration associated with the uranium Nopal 1 deposit, Chihuahua, Mexico.* Geochemistry of the Earth's Surface and of Mineral Formation. Aix en Provence, France: 371-372.

Ildefonse, P., J.-P. Muller, B. Clozel, and G. Calas. 1990b. Study of two alteration systems as natural analogues for radionuclide release and migration. *Engineering Geology* 29:413-439.

Janeczek, J. and R.C. Ewing. 1992. Coffinitization - a mechanism for the alteration of spent fuel under reducing conditions. *Materials Research Society Symposium Proceedings v. 257.* Boston: Materials Research Society: 497-504.

Johnson, L.H. and D.W. Shoesmith. 1988. Spent Fuel. W. Lutze and R. C. Ewing, ed. *Radioactive Waste Forms for the Future.* New York: North-Holland: 635-698.

Kleykamp, H. 1972. Formation of phases and distribution of fission products in an oxide fuel. *Behavior and Chemical State of Irradiated Fuels, Proceedings of Panel, Vienna.* Vienna: International Atomic Energy Agency, STI/PUB/303: 157-166.

Kleykamp, H. 1979. The chemical state of LWR high-power rods under irradiation. *Journal of Nuclear Materials* 84:109-117.

Kleykamp, H. 1985. The chemical state of the fission products in oxide fuels. *Journal of Nuclear Materials* 131:221-246.

Leroy, J.L., B. Aniel, and B. Poty. 1987. *The Sierra Pena Blanca (Mexico) and the Meseta Los Frailes (Bolivia); the uranium concentration mechanisms in volcanic environment during hydrothermal processes.* International Colloquium on Concentration mechanisms of uranium in geological environments, Oct. 2-5, 1985. B. Poty and M. Pagel, eds. Nancy, France: 211-234.

Leslie, B.W., E.C. Pearcy, and J.D. Prikryl. 1992. *NRC high-level radioactive waste research at CNWRA January 1 through June 30, 1992: Geochemical Natural Analogs.* CNWRA 92-01S. San Antonio, TX: CNWRA.

Leslie, B.W., E.C. Pearcy, and J.D. Prikryl. 1993. Oxidative alteration of uraninite under hydrologically unsaturated conditions at Peña Blanca, Chihuahua, Mexico: contaminant transport and source term constraints for the proposed repository at Yucca Mountain, Nevada. C. Interrante and R. Pabalan, eds., *Scientific Basis for Nuclear Waste Management XVI.* Boston: Materials Research Society: 505-512.

Luo, S. and T.-L. Ku. 1991. U-series isochron dating: a generalized method employing total sample dissolution. *Geochimica et Cosmochimica Acta* 55:555-564.

Manaktala, H., B. Sagar, and E.C. Pearcy. 1991. *Technical considerations in modeling release of radionuclides from spent LWR fuels under a repository environment.* Focus '91. Las Vegas, Nevada: American Nuclear Society, Inc.: 285-292.

Muller, J.-P., P. Ildefonse, and G. Calas. 1990. Paramagnetic defect centers in hydrothermal kaolinite from an altered tuff in the Nopal uranium deposit, Chihuahua, Mexico. *Clays and Clay Mineralogy* 38:600-608.

Murphy, W.M. and E.C. Pearcy. 1992. Source-term constraints for the proposed repository at Yucca Mountain, Nevada, derived from the natural analog at Peña Blanca, Mexico. C. G. Sombret, ed. *Scientific Basis for Nuclear Waste Management XV.* Pittsburgh: Materials Research Society: 521-527.

Murphy, W.M., E.C. Pearcy, and P.C. Goodell. 1991. Possible analog research sites for the proposed high-level nuclear waste repository in hydrologically unsaturated tuff at Yucca Mountain, Nevada. B. Come and N. A. Chapman, eds. *Fourth Natural Analogue Working Group Meeting and Pocos de Caldas project final workshop, Pitlochry, Scotland, 18-22 June 1990, Final Report n° EUR 13014 EN.* Brussels: Commission of the European Communities: 267-276.

Pearcy, E.C. and W.M. Murphy. 1992. *Site Selection and Workplan Report for the Geochemical Natural Analog Research Project.* CNWRA 92-014. San Antonio, TX: CNWRA.

Pearcy, E.C., W.M. Murphy, R.T. Green, B.W. Leslie, and J.D. Prikryl. 1991. *Geochemical Natural Analogs: Report on Research Activities for Calendar Year 1991.* CNWRA 91-01A. San Antonio, TX: CNWRA.

Shoesmith, D.W. and S. Sunder. 1992. The prediction of nuclear fuel (UO2) dissolution rates under waste disposal conditions. *Journal of Nuclear Materials* 190:20-35.

Shoesmith, D.W., S. Sunder, M.G. Bailey, and G.J. Wallace. 1989. The corrosion of nuclear fuel (UO_2) in oxygenated solutions. *Corrosion Science* 29:1115-1128.

Smith, D.K., Jr. 1984. Uranium mineralogy. B. DeVivo, F. Ippolito, G. Capaldi, and P. R. Simpson, eds. *Uranium geochemistry, mineralogy, geology, exploration, and resources.* England: The Institution of Mining and Metallurgy: 43-88.

Sunder, S., D.W. Shoesmith, R.J. Lemire, M.G. Bailey, and G.J. Wallace. 1991. The effect of pH on the corrosion of nuclear fuel (UO_2) in oxygenated solutions. *Corrosion Science* 32:373-386.

Taylor, P., E.A. Burgess, and D.G. Owen. 1980. An x-ray diffraction study of the formation of beta-$UO_{2.33}$ on UO_2 pellet surfaces in air at 229 to 275°C. *Journal of Nuclear Materials* 88:153-160.

Thomas, L.E., O.D. Slagle, and R.E. Einziger. 1991. Nonuniform oxidation of LWR spent fuel in air. *Journal of Nuclear Materials* 184:117-126.

USDOC. 1965. *World Weather Records 1951-60, Vol. 1 North America.* Washington, D.C.: US Department of Commerce.

Waber, N., H.D. Schorscher, and T. Peters. 1991. *Mineralogy, petrology and geochemistry of the Poços de Caldas analogue study sites, Minas Gerais, Brazil I. Osamu Utsumi uranium mine.* Report No. 2. Switzerland: NAGRA/SKB/UKDOE/USDOE.

Wilson, C.N. 1990a. *Results from NNWSI series 2 bare fuel dissolution tests.* PNL-7169 UC-802. Richland, Washington: Pacific Northwest Laboratory.

Wilson, C.N. 1990b. *Results from NNWSI series 3 spent fuel dissolution tests.* PNL-7170. Richland, Washington: Pacific Northwest Laboratory.

Wilson, C.N. 1991. Results from long-term dissolution tests using oxidized spent fuel. T. A. Abrajano Jr. and L. H. Johnson, ed. *Scientific Basis for Nuclear Waste Management XIV, Materials Research Society Symposium Proceedings Volume 212.* Boston, Massachusetts: Materials Research Society: 197-204.

Wilson, C.N. and C.J. Bruton. 1989. *Studies on spent fuel dissolution behaviour under Yucca Mountain repository conditions.* UCRL - 100223. Livermore, CA: Lawrence Livermore National Laboratory (LLNL).

Woodley, R.E. 1983. *The characteristics of spent LWR fuel relevant to its storage in geologic repositories.* Hanford Engineering Development Laboratory, HEDL-TME 83-28, UC-70.

Wronkiewicz, D.J., J.K. Bates, T.J. Gerding, E. Veleckis, and B.S. Tani. 1992. Uranium release and secondary phase formation during unsaturated testing of UO_2 at 90°C. *Journal of Nuclear Materials* 190:107-127.